Stability of Rate and Power Control Algorithms in Wireless Cellular Networks

Anders Möller and Ulf T. Jönsson
Royal Institute of Technology
[amolle,ulfj]@math.kth.se
Mats Blomgren and Fredrik Gunnarsson
Ericsson Research
[mats.blomgren,fredrik.gunnarsson]@ericsson.com

***Abstract*— In radio resource management for cellular networks a trade-off has to be made between the congestion level, related to cell coverage and intercell interference, and the Quality of Service (QoS), or data rates of the users. Herein this is implemented by using a fast inner power control loop and an outer rate control algorithm, working on a slower time scale.**

Due to the distributed nature of the network, both information and control is distributed. Measurements of congestion and QoS are used in the control loops and this introduces a nonlinear feedback. Another complicating factor is that filtering, computations and information exchange in the network introduce time delays.

In this paper we propose a general high order model as a cascade system with an outer and inner control loop. The control algorithms use distributed information available in the network. The full system model includes the nonlinear feedback from congestion and QoS measurements, time delays and time-scale modelling. We provide sufficient conditions for stability and convergence of the system. Our primary analysis tool is input output theory.

I. Introduction

We consider uplink in a WCDMA (Wideband Code Division Multiple Access) cellular network. WCDMA is currently undergoing a strong expansion globally and will remain the main provider of cellular data traffic for many years. The demand for high and stable throughput for data users increases constantly and this entails a challange to allocate and control the radio resourses efficiently.

To maintain the Quality of Service (QoS) of the users and to control congestion in the network, there are several control loops in wireless cellular networks. In the WCDMA standard, the users transmit on the same channel using orthogonal codes. In uplink, however, part of the orthogonality is lost. This causes an important feedback interconnection between the users for the control loops regulating on congestion and QoS. A fast distributed inner power control loop is used to ensure that the QoS is maintained under rapidly changing radio and interference conditions. By updating the transmission powers of the users, the inner power control loop tracks a reference value of the Signal to Interference Ratio (SIR), which is related to the QoS and data rate. The reference SIR-value is set by a slower outer rate control loop, which makes sure that the cell coverage is maintained by tracking a congestion reference. The outer loop works on a slower time scale, but the joint dynamics cannot be neglected.

An important motivation for using an outer control loop is to prevent power rushes, where the transmission powers of the users heavily increase. It is well known that if the SIR-target value is set too high, there exist no positive transmission powers such that the target SIR is achieved. The users will then compete with increasing transmission powers. In e.g. [16], [17] and [19] it was also shown that power rushes can be caused in the inner loop by too aggressive control algorithms in combination with delay. In e.g. [11] it was shown that by using a Smith predictor it is possible to compensate for delay. Typically there are delays both in the inner and outer control loop, which motivates the use of higher order control laws.

While the fast power control loop has been extensively studied over the last two decades, the outer loop has drawn less attention. Previous works concern mostly the aspect of rate allocation and have often used an optimization approach, see e.g. [5], [6], [9], [13], [14], [15] and [22]. In [15] convergence of distributed algorithms was studied, but only when assuming that the control loops work on different time scales. Joint dynamics for a type of outer loop algorithms were studied in [1] and [20]. Both considered a simplified linear system model, treating the nonlinear effects of interference and congestion feedback as additive disturbances.

The main contribution of this paper is the modelling and analysis of the joint dynamics of the two control loops. We derive the system model in a control theoretic framework and consider conditions for feasibility of the joint system. We also perform a general stability analysis using input output tools. Sufficient conditions are given for stability and convergence of the system. Then we focus on local analysis, where the problem structure is exploited. In particular we use scaling multipliers to sharpen the results from the previous section. This reveals a similar structure of the nonlinearities in the inner and outer loop.

The gains of using an outer loop are illustrated by simulations and analysis. In particular we show that power rushes can be prevented and we model a realistic scenario of a WCDMA network with delays and time-scale difference.

Anders Möller is supported by the Center for Industrial and Applied Mathematics (CIAM). Ulf T. Jönsson is supported by the Swedish Research Council (VR) and the ACCESS Linnaeus Centre at KTH.

The outline of the paper is as follows. In Section II we define the setting of the problem and in Section III the system model is derived. Equilibrium conditions are studied in Section IV and in Section V we analyze the relation between congestion and rate. This is followed by our main stability results in Section VI and VII. In Section VIII we consider examples and present simulations. The paper is concluded in Section IX.

II. System model and definitions

Consider a network with n mobiles transmitting to n receivers at base stations. The base stations could be common for different users or just operating a single mobile. An example is shown in Figure 1. Let the channel gain between transmitter j and receiver i be denoted by $\bar{g}_{ij}$. Assume that $\bar{g}_{ij} \geq 0, \forall (i,j)$ and $\bar{g}_{ii} > 0, \forall i$. Define the channel gain matrix $\bar{G}$ by $\bar{G} := [\bar{g}_{ij}]_{i,j=1}^{n}$. Define also the matrix $\bar{F}$ componentwise by

$$\bar{F}_{ij} := \begin{cases} 0, & i = j, \\ \bar{g}_{ij}, & i \neq j, \end{cases} \tag{1}$$

and $\bar{\Delta}$ as the diagonal matrix with $\bar{g}_{ii}$ in the diagonal element i, and let $g := [\ln(\bar{g}_{11}), \ldots, \ln(\bar{g}_{nn})]^T$.

Define $\bar{p}_i$ as the transmission power of user i and $\bar{p} := [\bar{p}_1, \ldots, \bar{p}_n]^T$. We similarly denote the background noise of receiver i by $\bar{\sigma}_i^2$ and $\bar{\sigma}^2 := [\bar{\sigma}_1^2, \ldots, \bar{\sigma}_n^2]^T$. The Signal to Interference Ratio (SIR) of user i, measured at receiver i, is

$$\bar{\gamma}_i := \frac{\bar{g}_{ii}\bar{p}_i}{\sum_{j \neq i} \bar{g}_{ij}\bar{p}_j + \bar{\sigma}_i^2} \tag{2}$$

and $\bar{\gamma} := [\bar{\gamma}_1, \ldots, \bar{\gamma}_n]^T$. The data rate of a user is related to its SIR by the Shannon capacity formula $\log(1 + \bar{\gamma}_i)$. The target SIR is defined by $\bar{\gamma}^\dagger := [\bar{\gamma}_1^\dagger, \ldots, \bar{\gamma}_n^\dagger]^T$.

The Rise over Thermal (RoT) is a measure of the congestion of a cellular network. It can be measured in the receiver and it is common to have constraints on the RoT-level, typically $\overline{RoT}_i[t] \leq \overline{RoT}_i^{\max}$, where $\overline{RoT}_i^{\max}$ is the maximum RoT of user i. The motivation behind this constraint is that the congestion is related to the coverage of the cell. By limiting the congestion it is possible for new users to enter the cell, see e.g. [15]. The total load at receiver i, here denoted by $\bar{L}_i^{tot}$, is defined as

$$\bar{L}_i^{tot} := \frac{\sum_{j=1}^{n} \bar{g}_{ij}\bar{p}_j}{\sum_{j=1}^{n} \bar{g}_{ij}\bar{p}_j + \bar{\sigma}_i^2},$$

and it is related to the RoT through the relation $\bar{L}_i^{tot} = 1 - \frac{1}{\overline{RoT}_i}$. Define the target total load, $\bar{L}^\dagger := [\bar{L}_1^\dagger, \ldots, \bar{L}_n^\dagger]^T$, by

$$\bar{L}_i^\dagger := 1 - \frac{1}{\overline{RoT}_i^\dagger},$$

where $\overline{RoT}_i^\dagger$ is the target RoT. For notational convenience we also introduce the diagonal matrix $\tilde{L}^\dagger$ with the diagonal entries $\bar{L}_i^\dagger$.

We use the notation $\text{diag}_i(x_i)$ to denote the diagonal matrix with x_i in the diagonal elements, and we let M^i denote the i:th row of a matrix M. We will frequently use both linear and logarithmic scale. For clarity we use the convention $\bar{x}$ to denote linear scale and x to denote logarithmic scale of a variable or constant x, e.g. $x = \ln(\bar{x})$. Let $\sigma(M)$ denote the spectrum and $\rho(M)$ denote the spectral radius of a matrix M. We say that a matrix, M, is non-negative if $M_{ij} \geq 0, \forall i,j$ and that a vector, x, is non-negative if $x_i \geq 0, \forall i$. Similarly we say that a matrix or vector is positive if $M_{ij} > 0, \forall i,j$, or $x_i > 0, \forall i$.

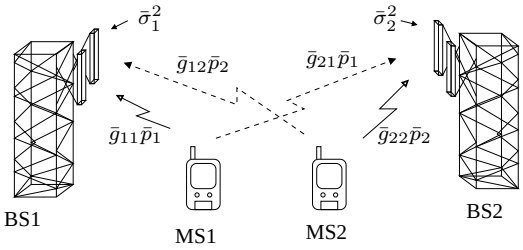

Fig. 1. Example of network setting.

III. Inner and Outer control algorithms

In a cellular system the channel gains and the system parameters constantly change and there are disturbances and uncertainties. This means that the system never reaches equilibrium and this motivates the use of control strategies to ensure system performance. In this section we model the control loops that ensure that the congestion is limited and the desired QoS achieved.

The system model can be seen as a cascade control system with an inner and outer control loop, see Figure 2. The model includes high order dynamics. This makes it possible to model time delays, filters and high order control algorithms. Furthermore, in real applications of cellular systems there is a time-scale difference between the loops. We show that this can be modelled by a high order outer loop controller.

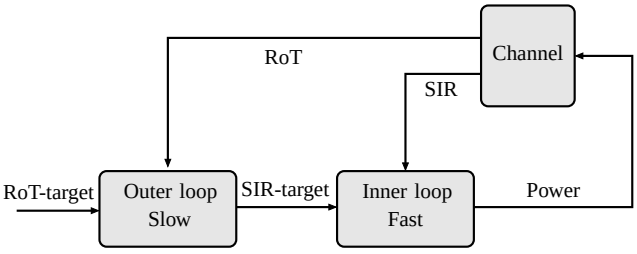

Fig. 2. Scheme over functionality of the outer and inner power control loops. The outer loop controls congestion by setting the SIR-target to the inner loop. The inner loop controls the SIR-level by changes in the transmission powers.

A. Inner loop

Power control algorithms for the inner loop has been extensively studied, see e.g. [8] [10] [11] [16] [19] [21]. Foschini and Miljanic proposed the SIR-based Distributed

Power Control (DPC) algorithm [8], defined by

$$\bar{p}_i[t+1] := \frac{\bar{\gamma}_i^\dagger}{\bar{\gamma}_i[t]}\bar{p}_i[t], \tag{3}$$

where $\bar{\gamma}_i^\dagger$ is the SIR-target. Assuming that the base station knows the actual transmission power of the mobile, the DPC-algorithm in (3) can be written as a linear system and easily analysed. However, in many real networks the feedback control is kept to a minimum. This means that the information exchange in the network must be distributed and the base station can typically only measure the power received, $\bar{g}_{ii}\bar{p}_i(t)$, not the individual terms.

By introducing logarithmic variables we can rewrite (3) such that the distributed nature of the information exchange is clarified. Indeed, with $p_i[t] := \ln(\bar{p}_i[t])$ and $\gamma_i^\dagger := \ln(\bar{\gamma}_i^\dagger)$, we can rewrite (3) as

$$p_i[t+1] = p_i[t] + (\gamma_i^\dagger - \gamma_i[t]) \tag{4}$$

where

$$\gamma_i[t] := \ln(\bar{\gamma}_i[t]) = \ln(\bar{g}_{ii}\bar{p}_i[t]) - \ln\Big(\sum_{j\neq i}\bar{g}_{ij}\bar{p}_j[t] + \bar{\sigma}_i^2\Big).$$

By using the time-shift operator q, defined by $qp_i[t] := p_i[t+1]$, we may rewrite (4) on input output form as $p_i[t] = R(q)(\gamma_i^\dagger - \gamma_i[t])$, where $R(q) = \frac{1}{q-1}$.

A challenge in control of cellular networks is to maintain robustness to delays. In e.g. [3], [4] and [23] it has been shown that the DPC-algorithm converges for any transmission delay of the interfering powers. However, in a cellular system there are typically no large transmission delays, but there are delays due to measuring, filtering, computations and control signalling to the mobile user. These delays can be modelled and are crucial for system stability. For example, a computational delay of size one can be modelled by $R(q) = \frac{1}{q(q-1)}$. The resulting system is then of higher order and is most conveniently modelled in the logarithmic scale. We consider high order inner power control algorithms of the general form

$$p_i[t] := K_{i,1}(q)\Big(\gamma_i^\dagger - g_{ii} + \ln\Big(\sum_{j\neq i}\bar{g}_{ij}\bar{p}_j[t] + \bar{\sigma}_i^2\Big)\Big), \tag{5}$$

where $g_{ii} := \ln(\bar{g}_{ii})$, $K_{i,1}(q) := \frac{R_i(q)}{1+R_i(q)}$, which we assume to be stable, and $R_i(q) := \frac{b_{i,1}(q)}{a_{i,1}(q)}$, where $a_{i,1}(q)$ and $b_{i,1}(q)$ are polynomials in q and $a_{i,1}(q)$ is a stable polynomial. For the DPC-algorithm in (4) we obtain the above form by using that $\ln(\bar{g}_{ii}\bar{p}_i[t]) = g_{ii} + p_i[t]$ and by taking $R_i(q) = \frac{1}{q-1}$. The distributed nature of the inner loop is illustrated within the dotted lines in Figure 3.

Remark 1: Given that $R_i(q)$ has an integrator, i.e. a term $\frac{1}{q-1}$, the experienced SIR will be equal to the target SIR in the equilibrium. If there is no integrator, the equilibrium SIR will be different from the reference value given by the outer loop. The steady state properties are not affected, since we will require an integrator in the outer loop. However, pole placement in the inner loop can be used to enhance performance.

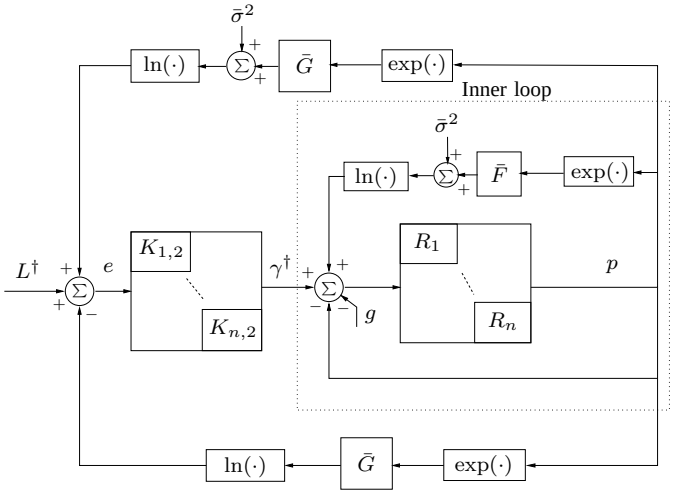

Fig. 3. Outer and inner loop in block diagram.

B. Outer loop

The outer loop controls on the total load as congestion measure and dynamically sets the reference value to the inner power control loop. When the inner loop has an integrator, the reference value can be interpreted as the target SIR, see Remark 1. Therefore we use that notation in the following derivations.

We begin by defining a first order update algorithm, which we later extend to include delays and higher order control laws, analogously to the inner loop model. Consider the update algorithm for $\bar{\gamma}_i^\dagger$ in linear scale given by

$$\bar{\gamma}_i^\dagger[t+1] = \frac{\bar{L}_i^\dagger}{\bar{L}_i^{tot}[t]}\bar{\gamma}_i^\dagger[t],$$

i.e. similar to the DPC-algorithm, but with the difference that now the experienced total load is compared to the target total load. In logarithmic scale the update algorithm can be written as

$$\gamma_i^\dagger[t+1] = \gamma_i^\dagger[t] + L_i^\dagger - L_i^{tot}[t],$$

where $L_i^\dagger := \ln(\bar{L}_i^\dagger)$ and

$$L_i^{tot}[t] = \ln\Big(\sum_{j=1}^{n}\bar{g}_{ij}\bar{p}_j[t]\Big) - \ln\Big(\sum_{j=1}^{n}\bar{g}_{ij}\bar{p}_j[t] + \bar{\sigma}_i^2\Big).$$

Similarly as for the inner power control loop, we consider higher order control algorithms on the following general form

$$\gamma_i^T[t] := K_{i,2}(q)e_i[t],$$

where $K_{i,2}(q) := \frac{b_{i,2}(q)}{(q-1)a_{i,2}(q)}$, and $a_{i,2}(q)$ and $b_{i,2}(q)$ are polynomials in q, $a_{i,2}(q)$ assumed to be a stable polynomial, and where $e_i[t] := L_i^\dagger - L_i^{tot}[t]$.

The intuitive idea of controlling on total load is that if the powers increase, the total load will increase above the reference value, which will decrease the target SIR, leading to lower powers. Similarly, if the powers are low, higher

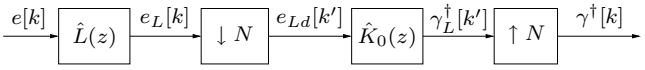

Fig. 4. Modelling of time-scale difference. A low-pass filter $\hat{L}(z)$ is first applied for anti-aliasing. It is followed by downsampling, the outer loop controller and finally upsampling.

powers can be allowed, raising the target SIR and eventually the powers.

The joint system model in logarithmic scale is illustrated in the block diagram in Figure 3. Note that filters for measured signals in both the inner and outer loop easily can be included in this framework, but for clarity this is omitted.

C. Time-scale difference

In the joint system we assume that there are two rates. A faster rate, on which the inner power control loop works, and a slower rate, on which the outer loop works. Furthermore, we assume that the error, $e[t] = L^\dagger - L^{tot}[t]$, is computed at the higher rate, as it is sampled at the base station. This can be modelled by a chain of operations containing a low-pass filter, downsampling, control and upsampling. This is illustrated in Figure 4.

A low-pass filter is needed to avoid aliasing and the cut-off frequency should be chosen near the Nyquist frequency. Downsampling reduces the data rate by selecting every N:th sample out of the filtered signal. The outer loop controller then works on this reduced data rate. After the controller the rate is again upsampled by sample and hold. This implies that the output signal of the controller is set constant for N time steps of the faster rate.

To include this in our model we consider the z-transforms of the operations. Let the low-pass filter be linear and causal and with the impulse response

$$L(q) := \sum_{k=0}^{\infty} L[k]q^{-k}.$$

If we let the filtered error be denoted by $e_L[k]$, we have

$$e_L[k] = \sum_{l=0}^{k} L[k-l]e[l].$$

The filtered error signal is now downsampled by taking every N:th sample to the signal $e_{Ld}[k']$. We then have

$$e_{Ld}[k'] = e_L[k'N] = \sum_{l=0}^{k'N} L[k'N-l]e[l], \quad \forall k'.$$

Let the z-transforms of L, e_L and e_{Ld} be denoted by $\hat{L}(z)$, $\hat{e}_L(z)$ and $\hat{e}_{Ld}(z)$. We have

$$\begin{aligned}
\hat{e}_{Ld}(z) &= \sum_{k'=0}^{\infty} e_{Ld}[k']z^{-k'} \\
&= \sum_{k'=0}^{\infty}\sum_{l=0}^{k'N} L[k'N-l]e[l]z^{-k'} \\
&= \sum_{k'=0}^{\infty}\sum_{l=0}^{k'N} L[k'N-l]z^{-(k'N-l)/N}e[l]z^{-l/N} \\
&= \sum_{l=0}^{\infty}\sum_{k'=\lceil l/N\rceil}^{\infty} L[k'N-l]z^{-(k'N-l)/N}e[l]z^{-l/N} \\
&= \left\{m = k'N - l\right\} \\
&= \sum_{l=0}^{\infty}\sum_{m=0}^{\infty} L[m]z^{-m/N}e[l]z^{-l/N} \\
&= \sum_{l=0}^{\infty} e[l]z^{-l/N}\sum_{m=0}^{\infty} L[m]z^{-m/N} \\
&= \hat{L}(z^{1/N})\hat{e}(z^{1/N}),
\end{aligned}$$

where $\lceil\cdot\rceil$ is the ceiling function that rounds up to the lowest following integer. Denote the outer loop controller on the slower time-scale by $\hat{K}_0(z)$ and the SIR-target output on the slow rate by $\gamma_L^\dagger[k']$. It is then given by

$$\hat{\gamma}_L^\dagger(z) = \hat{K}_0(z)\hat{L}(z^{1/N})\hat{e}(z^{1/N}).$$

The final step is upsampling by sample and hold. Denote the z-transform of the SIR-target on the fast time-scale by $\hat{\gamma}^\dagger(z)$. We get

$$\begin{aligned}
\hat{\gamma}^\dagger(z) &= \sum_{k=0}^{\infty}\gamma^\dagger[k]z^{-k} \\
&= \sum_{k'=0}^{\infty}\gamma_L^\dagger[k']\left(\sum_{k''=k'N}^{(k'+1)N-1} z^{-k''}\right) \\
&= \sum_{k'=0}^{\infty}\gamma_L^\dagger[k']z^{-k'N}\left(\frac{1-z^{-N}}{1-z^{-1}}\right) \\
&= \hat{\gamma}_L^\dagger(z^N)\left(\frac{1-z^{-N}}{1-z^{-1}}\right).
\end{aligned}$$

Finally we arrive at the compound transfer function including all operations

$$\hat{K}_2(z) = \hat{K}_0(z^N)\hat{L}(z)\left(\frac{1-z^{-N}}{1-z^{-1}}\right).$$

Note that the derivation is based on the assumption that the filter is ideal so that no aliasing occur.

Consider a simple outer loop controller with an integrator, e.g. $\hat{K}_0(z) = \frac{K_I}{z-1}$, where K_I is a constant. This results in the transfer function

$$\hat{K}_2(z) = \frac{K_I}{z^{N-1}(z-1)}\hat{L}(z),$$

i.e. an integrator with an additional delay of $N-1$ samples and the low-pass filter. The cut-off frequency of the low-pass filter should be near the Nyquist frequency $w_s = \frac{\pi}{N}$. We observe that if we assume no low-pass filter and no time-scale difference, i.e. $N = 1$, we recover the original outer loop controller by substituting z with q. We will use the notation $K_2(q)$ for the outer loop control, which may then include modelling of time-scale differences.

IV. Equilibrium point

In this section we study conditions for a unique equilibrium point and its properties for the system model introduced in the previous section.

Proposition 1: In the equilibrium it holds that $\bar{L}_i^\dagger = \bar{L}_i^{tot}$ for all users i.

Proof: A proof is given in the appendix. ∎

Proposition 2: Assume that $\bar{L}_i^\dagger < 1, \forall i$, and that $\bar{G}^{-1}$ exists. Recall that $\tilde{L}^\dagger = \text{diag}_i(\bar{L}_i^\dagger)$. Then the unique equilibrium powers, $\bar{p}^*$, are given by

$$\bar{p}^* = ((I - \tilde{L}^\dagger)\bar{G})^{-1}\tilde{L}^\dagger\bar{\sigma}^2.$$

A sufficient and necessary condition for finite non-negative powers is

$$\bar{G}^{-1}\begin{bmatrix} \frac{\bar{L}_1^\dagger}{1-\bar{L}_1^\dagger}\bar{\sigma}_1^2 \\ \vdots \\ \frac{\bar{L}_n^\dagger}{1-\bar{L}_n^\dagger}\bar{\sigma}_n^2 \end{bmatrix} \geq 0. \tag{6}$$

Proof: Using Proposition 1 we have

$$\begin{aligned}
\bar{L}_i^{tot}(t) = \bar{L}_i^\dagger \quad \forall i \quad &\Leftrightarrow \\
\frac{\sum_{j=1}^n \bar{g}_{ij}\bar{p}_j}{\sum_{j=1}^n \bar{g}_{ij}\bar{p}_j + \bar{\sigma}_i^2} = \bar{L}_i^\dagger \quad \forall i \quad &\Leftrightarrow \\
\sum_{j=1}^n \bar{g}_{ij}\bar{p}_j = \bar{L}_i^\dagger\left(\sum_{j=1}^n \bar{g}_{ij}\bar{p}_j + \bar{\sigma}_i^2\right) \quad \forall i \quad &\Leftrightarrow \\
(1-\bar{L}_i^\dagger)\sum_{j=1}^n \bar{g}_{ij}\bar{p}_j = \bar{L}_i^\dagger\bar{\sigma}_i^2 \quad \forall i \quad &\Leftrightarrow \\
(1-\bar{L}_i^\dagger)\bar{G}^i\bar{p} = \bar{L}_i^\dagger\bar{\sigma}_i^2 \quad \forall i \quad &\Leftrightarrow \\
(I-\tilde{L}^\dagger)\bar{G}\bar{p} = \tilde{L}^\dagger\bar{\sigma}^2 \quad &\Leftrightarrow \\
\bar{p}^* = ((I-\tilde{L}^\dagger)\bar{G})^{-1}\tilde{L}^\dagger\bar{\sigma}^2 &
\end{aligned}$$

The condition for existence of non-negative powers can be written as $((I-\tilde{L}^\dagger)\bar{G})^{-1}\tilde{L}^\dagger\bar{\sigma}^2 \geq 0$, which can be rewritten to $\bar{G}^{-1}(I-\tilde{L}^\dagger)^{-1}\tilde{L}^\dagger\bar{\sigma}^2 \geq 0$. Since $(I-\tilde{L}^\dagger)$ is a diagonal matrix it can easily be inverted, giving $(I-\tilde{L}^\dagger)^{-1} = \text{diag}_i\left(\frac{1}{1-\bar{L}_i^\dagger}\right)$. Multiplying with $\tilde{L}^\dagger$ and $\bar{\sigma}^2$ we get a vector with elements $\frac{\bar{L}_i^\dagger}{1-\bar{L}_i^\dagger}\bar{\sigma}_i^2, \forall i$. Sufficient and necessary conditions for the existence of non-negative powers can hence be stated as in (6). Note that $\bar{G}^{-1}$ exists with probability one. ∎

Inspired by this we make the following definition.

Definition 1: The joint system is feasible if there exist finite non-negative powers corresponding to the target total load.

Note that feasibility of the system implies that the SIR of all users will be non-negative in the equilibrium. This follows since the powers and all system parameters are non-negative.

For the inner power control loop, feasibility is usually defined in terms of the target SIR and system parameters $\bar{\Delta}$ and $\bar{F}$. Feasibility of the inner power control loop also implies the existence of finite non-negative powers. Hence also the joint system feasibility can be guaranteed with the same condition. This is shown in the following proposition. First define the equilibrium SIR[1] of user i by $\bar{\gamma}_i^*$ and let $\bar{\Gamma}^* := \text{diag}_i(\bar{\gamma}_i^*)$.

Proposition 3: Assume that $\rho(\bar{\Gamma}^*\bar{\Delta}^{-1}\bar{F}) < 1$. Then the system is feasible and $\bar{L}_i^\dagger < 1, \forall i$.

Proof: A proof is given in the appendix. ∎

Note that the equilibrium total load is then implicitly determined by the choice of SIR-target. Note also that the converse of this proposition does not hold, i.e. there could be solutions to the equilibrium equation

$$\bar{p}^* = ((I - \tilde{L}^\dagger)\bar{G})^{-1}\tilde{L}^\dagger\bar{\sigma}^2,$$

where the power vector has negative components even though $\bar{L}_i^\dagger < 1, \forall i$.

This is shown in the following example.

Example 1: Let

$$\bar{G} = \begin{bmatrix} 1 & 0.01 & 0.01 \\ 0.01 & 1 & 0.01 \\ 0.01 & 0.01 & 1 \end{bmatrix}, \quad \bar{\sigma}^2 = \begin{bmatrix} 0.05 \\ 0.05 \\ 0.05 \end{bmatrix}.$$

Let the target total load be given by $\bar{L}_1^\dagger = 0.6667$ and $\bar{L}_2^\dagger = \bar{L}_3^\dagger = 0.9951$. This gives the equilibrium power and SIR vectors

$$\bar{p}^* = [-0.1,\ 10,\ 10]^T,\ \bar{\gamma}^* = [-0.6667,\ 0.9853,\ 0.9853]^T.$$

The system in the example is infeasible, since there are no non-negative powers giving the desired total load target. Furthermore the equilibrium SIR corresponding to the negative power is negative.

The following proposition shows that this is always the case.

Proposition 4: Assume that $\bar{L}_i^\dagger \in [0, 1), \forall i$. Then a negative element of the power vector corresponds to a negative SIR.

Proof: A proof is given in the appendix. ∎

Remark 2: Total load is a decentralized measure and global information is needed to avoid infeasibility. In Section VIII we will consider the properties of an infeasible system.

V. Congestion and QoS properties

In this section we show the relation between the total load, determining the congestion, and the SIR, determining the throughput, or QoS. Any feasible power vector corresponds to a total load and a SIR. Through the powers, for given system parameters, we obtain a relation between the total load and the SIR.

[1]Recall that if there is an integrator in the inner loop, the equilibrium SIR and the target SIR are equal.

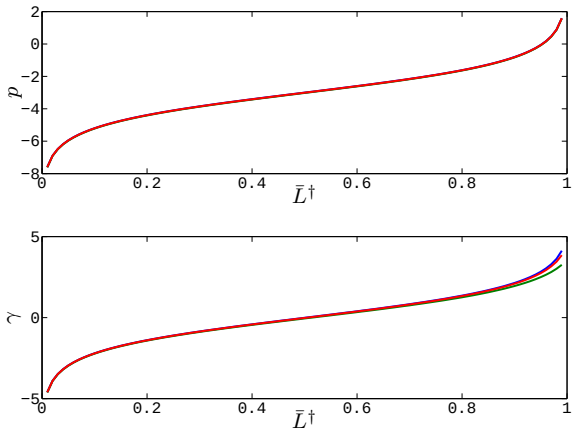

Fig. 5. The relation between total load target and transmission powers and SIR for an example. Note that the y-axis is in logarithmic scale, whereas the x-axis is in linear scale.

Example 2: Consider the system given by

$$\bar{G} = \begin{bmatrix} 1.0000 & 0.0010 & 0.0050 \\ 0.0250 & 1.0000 & 0.0025 \\ 0.0100 & 0.0010 & 1.0000 \end{bmatrix} \quad \text{and} \quad \bar{\sigma}^2 = \begin{bmatrix} 0.05 \\ 0.05 \\ 0.05 \end{bmatrix}.$$

In Figure 5 we can see the equilibrium power and SIR as functions of the total load target, which is set equal for all users. An increase in the total load target leads to an increase of the SIR and the transmission powers.

The example indicates that to maximize the throughput, the total load target should be chosen as high as possible. The following proposition confirms this rule of thumb.

Proposition 5:

$$\bar{\gamma}_i = \frac{\bar{L}_i^{tot} - \bar{K}_i}{1 - \bar{L}_i^{tot}} \quad \text{and} \quad \bar{L}_i^{tot} = \frac{\bar{\gamma}_i + \bar{K}_i}{\bar{\gamma}_i + 1},$$

where $\bar{K}_i$ is given by

$$\bar{K}_i := \frac{\sum_{j \neq i} \bar{g}_{ij} \bar{p}_j}{\sum_{j \neq i} \bar{g}_{ij} \bar{p}_j + \bar{\sigma}_i^2}. \tag{7}$$

In e.g. [19] K_i was shown relate to stability of the inner power control loop.

Proof: A proof is given in the appendix. ■

The relation between the total load target and the SIR is however not always intuitive. This is due to the nonlinear relation through the equilibrium powers. The following example illustrates how an increase of the total load target for one user leads to an increased SIR for the same user, but to the cost of a larger decrease of the SIRs for the other users.

Example 3: Let

$$\bar{G} = \begin{bmatrix} 1.0000 & 0.5500 & 0.0050 \\ 0.4000 & 1.0000 & 0.4000 \\ 0.0100 & 0.5500 & 1.0000 \end{bmatrix} \quad \text{and} \quad \bar{\sigma}^2 = \begin{bmatrix} 0.05 \\ 0.05 \\ 0.05 \end{bmatrix}.$$

First consider using the target total load $\bar{L}_i^{\dagger_1} = 0.8, \forall i$. This gives the equilibrium powers and SIRs

$$\bar{p}^1 = [0.1590, 0.0731, 0.1582]^T \quad \text{and}$$
$$\bar{\gamma}^1 = [1.7469, 0.4135, 1.7230]^T.$$

Let the sum of the Shannon capacities be a measure of the joint throughput. Then the throughput is equal to 0.2188.

Now consider increasing the total load of user two. Let the new assignment of total load be given by $\bar{L}_1^{\dagger_2} = \bar{L}_3^{\dagger_2} = 0.8$ and $\bar{L}_2^{\dagger_2} = 0.82$. The new equilibrium powers and SIRs are given by

$$\bar{p}^2 = [0.1320, 0.1224, 0.1313]^T \quad \text{and}$$
$$\bar{\gamma}^2 = [1.1186, 0.7883, 1.1068]^T.$$

We note that the SIR of user two has increased, and that the SIRs of the other two users have decreased. The new throughput is -0.0243, which is lower than for the original total load target assignment.

The exact relation between total load and SIR is given in the following proposition.

Proposition 6: Assume that the system is feasible with respect to a given SIR, $\bar{\Gamma}^*$. Then the target total load, $\bar{L}^\dagger$, is positive and is given componentwise by

$$\bar{L}_i^\dagger = \frac{\bar{M}^i \bar{\sigma}^2}{(I + \bar{M})^i \bar{\sigma}^2},$$

where $\bar{M} := \bar{G}(I - \bar{\Gamma}^* \bar{\Delta}^{-1} \bar{F})^{-1} \bar{\Gamma}^* \bar{\Delta}^{-1}$.

Assume that the system is feasible for a given total load, $\bar{L}^\dagger$. Then the SIR, $\bar{\Gamma}^*$, is positive and is given componentwise by

$$\bar{\gamma}_i^* = \frac{\bar{N}^i \bar{\sigma}^2}{(\bar{\Delta}^{-1} + \bar{\Delta}^{-1} \bar{F} \bar{N})^i \bar{\sigma}^2},$$

where $\bar{N} := ((I - \tilde{L}^\dagger)\bar{G})^{-1} \tilde{L}^\dagger$.

Proof: A proof is given in the appendix. ■

VI. Stability Analysis

The stability analysis in this section is of a rather general form and we discuss more about the problem structure and study some important examples in more detail in a later section. We first rewrite the system to a more compact form. Then we consider the resulting blocks as operators on a Banach space and apply Lipschitz analysis to obtain sufficient conditions for stability and convergence of the system.

The analysis is made using logarithmic scale and is based on the existence of an equilibrium point, p^*. We consider the dynamics of deviations around the equilibrium point, $z = p - p^*$ and disturbances δr.

The full system model, depicted as a block diagram in Figure 3, can equivalently be rewritten into the system in Figure 6, where an artificial lower and upper loop is added with gain C, where $C = \text{diag}_i(C_i)$. This results in Φ^{out} being dependent of C. Note that this way of rewriting the

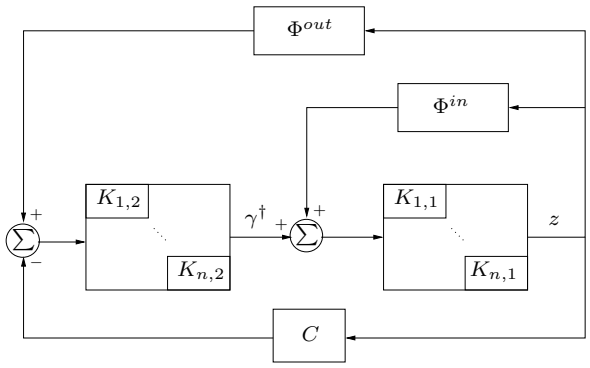

Fig. 6. Rewritten block diagram of joint outer and inner loop with an artificial lower loop with gain C.

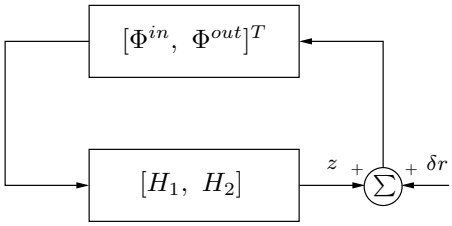

Fig. 7. Input output form of the joint system.

system is only for analysis purpose. We have used the following notation.

$$\Phi^{out}(z) := [\Phi_1^{out}(z), \ldots, \Phi_n^{out}(z)]^T$$
$$\Phi^{in}(z) := [\Phi_1^{in}(z), \ldots, \Phi_n^{in}(z)]^T$$
$$\Phi_i^{out}(z) := \ln\left(\frac{\sum_{j=1}^n \bar{g}_{ij} e^{p_j^*} e^{z_j} + \bar{\sigma}_i^2}{\sum_{j=1}^n \bar{g}_{ij} e^{p_j^*} e^{z_j}}\right) + C_i z_i + L_i^\dagger$$
$$\Phi_i^{in}(z) := \ln\left(\sum_{j\neq i}^n \bar{g}_{ij} e^{p_j^*} e^{z_j} + \bar{\sigma}_i^2\right) - \gamma_i^\dagger(p^*) - g_{ii} - p_i^*$$
$$K_1(q) := \text{diag}_i(K_{i,1}) = \text{diag}_i(R_i(q)/(1+R_i(q)))$$
$$K_2(q) := \text{diag}_i(K_{i,2}).$$

We now further rewrite the system to input output form, see Figure 7, where

$$H_1(q) := (I + K_1(q)K_2(q)C)^{-1}K_1(q)$$
$$H_2(q) := (I + K_1(q)K_2(q)C)^{-1}K_1(q)K_2(q).$$

The analysis will be performed in the following signal spaces

(i) $l_\infty^n := \{z : \mathbb{N} \to \mathbb{R}_\infty^n : \|z\|_\infty < \infty\}$
(ii) $l_{2,\infty}^n := \{z : \mathbb{N} \to \mathbb{R}_\infty^n : \|z\|_{2,\infty} < \infty\}$

where the norms are defined as $\|z\|_\infty := \sup_k |z[k]|_\infty$ and $\|z\|_{2,\infty} := (\sum_{k=0}^\infty |z[k]|_\infty^2)^{1/2}$. The spatial dimension will often be suppressed. It has previously been established that use of the l_2-space is not appropriate for this kind of analysis, see e.g. [17] or [18] for a further discussion on choice of signal spaces.

Let F be a nonlinear operator $F : X \to X$ such that $F(0) = 0$ and X is a normed vector space. Then the global Lipschitz constant is defined as

$$L[F; X] := \sup_{z_1,z_2\in X, z_1\neq z_2} \frac{\|F(z_1) - F(z_2)\|_X}{\|z_1 - z_2\|_X},$$

where $\|\cdot\|_X$ denotes the norm on X. For us it will be interesting to consider the Lipschitz constant on a subset B_X of X defined by how large deviations around the equilibrium we consider. Define

$$L[F; B_X] := \sup_{z_1,z_2\in B_X, z_1\neq z_2} \frac{\|F(z_1) - F(z_2)\|_X}{\|z_1 - z_2\|_X}.$$

For linear operators the gain and Lipschitz constants coincide. The l_1-norm of a linear system H_i is defined as

$$\|H_i\|_1 := \sum_{k=0}^\infty |h_i[k]|,$$

where $h_i[k]$ is the impulse response at time k. For a diagonal matrix H, $H(q) = \text{diag}_i(H_i)$, the induced norms from l_∞ and $l_{2,\infty}$ become (see e.g. [7])

$$\|H\|_{l_\infty\to l_\infty} = \|H\|_1 := \max(\|H_1\|_1, \ldots, \|H_n\|_1)$$
$$\|H\|_{l_{2,\infty}\to l_{2,\infty}} \leq \|H\|_{1,1} := \sum_{k=0}^\infty |h[k]|_1,$$

where we used the matrix norm $|M|_1 = |M|_{\mathbb{R}_\infty^n\to\mathbb{R}_\infty^n} = \max_{1\leq i\leq n}\sum_{j=1}^n |M_{ij}|$. Clearly $\|H\|_1 \leq \|H\|_{1,1}$, and equality holds if $H_i = H_j, \forall(i,j)$.

Let X be either of the spaces l_∞^n or $l_{2,\infty}^n$. Consider the set $B \in \mathbb{R}^n$, defined componentwise by $p_i^{\min} \leq p_i \leq p_i^{\max}, \forall i$, where $p_i^{\min}, p_i^{\max}$ are lower and upper bounds on the transmission powers of the users. The induced sets for the deviations around the equilibrium point, z, are then given by

$$B^* := \{z \in \mathbb{R}_\infty^n : p_i^{\min} - p_i^* \leq z_i \leq p_i^{\max} - p_i^*, \forall i\} \quad (8)$$
$$B_X^* := \{z \in X : z[k] \in B^*, \forall k\}. \quad (9)$$

For our analysis we need to consider the maximum interior balls in B^* and B_X^*, which are defined as

$$B^*(\gamma) := \{z \in \mathbb{R}_\infty : |z|_\infty \leq \gamma\},$$
$$B_X^*(\gamma) := \{z \in X : z[k] \in B^*(\gamma),\ \forall k\},$$

where $\gamma := \min_i\{\min\{p_i^* - p_i^{\min}, p_i^{\max} - p_i^*\}\}$.

Proposition 7:

$$L[\Phi^{in}; B_{l_\infty}^*(\gamma)] = L[\Phi^{in}; B_{l_{2,\infty}}^*(\gamma)] = L[\Phi^{in}; B^*(\gamma)]$$
$$= \max_{z\in B^*(\gamma)} |\nabla\Phi^{in}(z)|_1$$
$$= \max_i \frac{\bar{F}^i e^{p^*+z^{\max}}}{\bar{\sigma}_i^2 + \bar{F}^i e^{p^*+z^{\max}}} < 1,$$

where $e^{p^*+z^{\max}} := [e^{p_1^*+z_1^{\max}}, \ldots, e^{p_n^*+z_n^{\max}}]$ and $z_i^{\max} := p_i^{\max} - p_i^*, \forall i$.

Proof: See [17] or [19]. ∎

Proposition 8:

$$L[\Phi^{out};B^*_{l_\infty}(\gamma)] = L[\Phi^{out};B^*_{l_{2,\infty}}(\gamma)] = L[\Phi^{out};B^*(\gamma)]$$
$$= \max_{z\in B^*(\gamma)} |\nabla\Phi^{out}(z)|_1$$
$$= \max_i \max_{z\in B^*(\gamma)} \left(\frac{\bar\sigma_i^2 \bar F^i e^{p^*+z}}{(\bar G^i e^{p^*+z}+\bar\sigma_i^2)(\bar G^i e^{p^*+z})} + \left| C_i - \frac{\bar\sigma_i^2 \bar g_{ii} e^{p_i^*} e^{z_i}}{(\bar G^i e^{p^*+z}+\bar\sigma_i^2)(\bar G^i e^{p^*+z})} \right| \right)$$

Proof: A proof is given in the appendix. ∎

Note that the Lipschitz constant depends on the value of the parameter C.

We are now ready for our main theorem on stability.

Theorem 1: Assume that

$$\|H_1\|_1 L[\Phi^{in};B^*(\gamma)] + \|H_2\|_1 L[\Phi^{out};B^*(\gamma)] < 1,$$

then there exists a unique power trajectory $z \in B^*_{l_\infty}(\gamma)$ for all

$$\begin{aligned}\|\delta r\|_\infty \le \gamma\Big(1 &- \|H_1\|_1 L[\Phi^{in};B^*(\gamma)] \\ &- \|H_2\|_1 L[\Phi^{out};B^*(\gamma)]\Big).\end{aligned} \tag{10}$$

If it in addition holds that $\|\delta r\|_{l_{2,\infty}} < \infty$ and that

$$\begin{aligned}&\|H_1\|_{l_{2,\infty}\to l_{2,\infty}} L[\Phi^{in};B^*(\gamma)] \\ &+ \|H_2\|_{l_{2,\infty}\to l_{2,\infty}} L[\Phi^{out};B^*(\gamma)] < 1,\end{aligned}$$

then $p[k] \to p^*$ as $k \to \infty$.

Proof: A proof is given in the appendix. ∎

Remark 3: In the analysis we rewrite the system by introducing the direct feedback with gain C to the system part of the block diagram, see Figure 6. This loop transformation is needed, since the l_1-norm of the integrator in K_2 is infinite.

VII. Scaling multipliers and local analysis

Structure of the problem can be understood by introducing scaling multipliers, see Figure 8. This gives the transformed but equivalent system where

$$\begin{aligned}\hat H_1(q) &:= D^{-1}H_1(q)D = H_1(q)\\ \hat H_2(q) &:= D^{-1}H_2(q)D = H_2(q)\\ \hat\Phi^{in}(\hat z) &:= D^{-1}\Phi^{in}(D\hat z)\\ \hat\Phi^{out}(\hat z) &:= D^{-1}\Phi^{out}(D\hat z)\\ \widehat{\delta r} &:= D^{-1}\delta r, \qquad \hat z := D^{-1}z\end{aligned}$$

for any $D \in \mathcal{D} := \{D = \mathrm{diag}_i(d_i) : d_i > 0\}$.

Proposition 9: The scaled nonlinearities $\hat\Phi^{in} : \mathbb{R}^n_\infty \to \mathbb{R}^n_\infty$ and $\hat\Phi^{out} : \mathbb{R}^n_\infty \to \mathbb{R}^n_\infty$ are Lipschitz on $D^{-1}B^* \subset \mathbb{R}^n_\infty$ with

$$L[\hat\Phi^{in};D^{-1}B^*] = \max_{z\in B^*} |D^{-1}\nabla\Phi^{in}(z)D|_1 := L^{in}_D$$

and

$$L[\hat\Phi^{out};D^{-1}B^*] = \max_{z\in B^*} |D^{-1}\nabla\Phi^{out}(z)D|_1 := L^{out}_D$$

Proof: A proof is given in the appendix. ∎

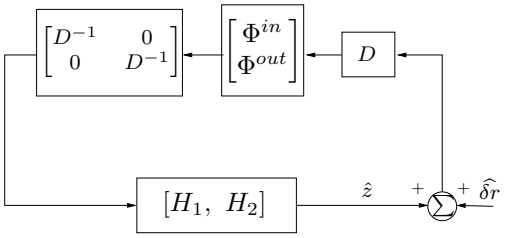

Fig. 8. Input output form of the joint scaled system.

To get to our stability result in the scaled signal space we need to consider the Lipschitz constants for the signal spaces previously defined. Define

$$\hat\gamma := \min_i \left\{ \min\left\{ \frac{1}{d_i}(p_i^* - p_i^{\min}), \frac{1}{d_i}(p_i^{\max} - p_i^*) \right\} \right\},$$

and the sets

$$\begin{aligned}C(\hat\gamma) &:= \{z \in \mathbb{R}_\infty : -d_i\hat\gamma \le z_i \le d_i\hat\gamma,\ \forall i\}\\ C_X(\hat\gamma) &:= \{z \in X : z[k] \in C(\hat\gamma),\ \forall k\}\\ C_{\delta,X}(\hat\gamma) &:= \Big\{\delta r \in X : |\delta r_i[k]| \le \hat\gamma d_i \Big(1 - \|H_1\|_1 L^{in}_D\\ &\qquad - \|H_2\|_1 L^{out}_D\Big), \forall (i,k)\Big\}\end{aligned}$$

Proposition 10: The scaled nonlinearities $\hat\Phi^{in} : X \to X$ and $\hat\Phi^{out} : X \to X$ are Lipschitz on $C_X(\hat\gamma)$ with

$$\begin{aligned}L[\hat\Phi^{in};C_{l_\infty}(\hat\gamma)] &= L[\hat\Phi^{in};C_{l_{2,\infty}}(\hat\gamma)] = L[\hat\Phi^{in};C(\hat\gamma)]\\ &\le \max_{z\in B^*} |D^{-1}\nabla\Phi^{in}(z)D|_1 = L^{in}_D\end{aligned}$$

and

$$\begin{aligned}L[\hat\Phi^{out};C_{l_\infty}(\hat\gamma)] &= L[\hat\Phi^{out};C_{l_{2,\infty}}(\hat\gamma)] = L[\hat\Phi^{out};C(\hat\gamma)]\\ &\le \max_{z\in B^*} |D^{-1}\nabla\Phi^{out}(z)D|_1 = L^{out}_D\end{aligned}$$

Proof: A proof can be found in [18] and [19]. ∎

We can now give conditions for stability.

Corollary 1: If

$$\|H_1\|_1 L^{in}_D + \|H_2\|_1 L^{out}_D < 1,$$

then there exists a unique power distribution $z \in C_{l_\infty}(\hat\gamma)$ for all $\delta r \in C_{\delta,l_\infty}(\hat\gamma)$.

If it in addition holds that $\|\delta r\|_{2,\infty} < \infty$ and

$$\|H_1\|_{l_{2,\infty}\to l_{2,\infty}} L^{in}_D + \|H_2\|_{l_{2,\infty}\to l_{2,\infty}} L^{out}_D < 1,$$

then $z[k] \to 0$ as $k \to \infty$.

Proof: We study stability in the scaled signal space, where $\hat z := D^{-1}z$. $z \in C_{l_\infty}(\hat\gamma)$ implies that $\hat z \in B^*_{l_\infty}(\hat\gamma)$ and $\delta r \in C_{\delta,l_\infty}(\hat\gamma)$ implies that

$$\|\widehat{\delta r}\|_\infty \le \hat\gamma\Big(1 - \|H_1\|_1 L^{in}_D - \|H_2\|_1 L^{out}_D\Big).$$

Theorem 1 then proves the statement. ∎

We can use more structure of the problem by an analysis of the nonlinearities around the equilibrium point. As a first step we study each nonlinearity by itself and then we show how they relate and how this can be used in the analysis. This will bring clarity and some intuition in how the system parameters

relate to stability and performance of the system. We also propose how to choose the scalings in the equilibrium point. Define

$$\bar{\gamma}_i(z) := \frac{\bar{g}_{ii}e^{p_i^*+z_i}}{\bar{\sigma}_i^2 + \bar{F}^i e^{p^*+z}} \quad \text{and} \quad \bar{\Gamma}(z) := \text{diag}_i(\bar{\gamma}_i(z)).$$

Proposition 11:

$$\nabla\Phi^{in}(z) = \text{diag}_i(e^{p_i^*+z_i})^{-1}\bar{\Gamma}(z)\bar{\Delta}^{-1}\bar{F}\text{diag}_i(e^{p_i^*+z_i})$$

and

$$\sigma(\nabla\Phi^{in}(z)) = \sigma(\bar{\Gamma}(z)\bar{\Delta}^{-1}\bar{F}).$$

Remark 4: In particular the result implies that in the equilibrium point, the Jacobian of the inner power control loop has the same eigenvalues as the matrix determining feasibility of the inner power control loop.

Proof: First note that

$$\bar{\gamma}_i(z) = \frac{\bar{g}_{ii}e^{p_i^*+z_i}}{\bar{\sigma}_i^2 + \bar{F}^i e^{p^*+z}} \quad \Leftrightarrow \quad \bar{\sigma}_i^2 + \bar{F}^i e^{p^*+z} = \frac{\bar{g}_{ii}e^{p_i^*+z_i}}{\bar{\gamma}_i(z)}.$$

We have

$$\nabla\Phi^{in}(z)_{ij} = \begin{cases} 0, & i = j, \\ \frac{\bar{g}_{ij}e^{p_j^*+z_j}}{\bar{\sigma}_i^2+\bar{F}^i e^{p^*+z}}, & i \neq j, \end{cases} = \begin{cases} 0, & i = j, \\ \frac{\bar{g}_{ij}}{\bar{g}_{ii}}\frac{e^{p_j^*+z_j}}{e^{p_i^*+z_i}}\bar{\gamma}_i(z), & i \neq j. \end{cases}$$

This can be written as

$$\nabla\Phi^{in}(z) = \text{diag}_i(e^{p_i^*+z_i})^{-1}\bar{\Gamma}(z)\bar{\Delta}^{-1}\bar{F}\text{diag}_i(e^{p_i^*+z_i}),$$

and hence $\nabla\Phi^{in}(z)$ is similar to $\bar{\Gamma}(z)\bar{\Delta}^{-1}\bar{F}$ and share the same eigenvalues. ∎

Now consider $\nabla\Phi^{out}$ in the equilibrium point, where $z = 0$, with the choice

$$C_i = \frac{\bar{\sigma}_i^2\bar{g}_{ii}e^{p_i^*}}{(\bar{G}^i e^{p^*} + \bar{\sigma}_i^2)(\bar{G}^i e^{p^*})}, \quad \forall i, \tag{11}$$

which implies that the diagonal elements of $\nabla\Phi^{out}(0)$ are cancelled.

Proposition 12:

$$\nabla\Phi^{out}(0) = \text{diag}_i\left(\frac{1}{e^{p_i^*}}\frac{\bar{L}_i^\dagger - 1}{\bar{L}_i^\dagger}\frac{\bar{\gamma}_i^*}{\bar{\gamma}_i^* + 1}\right)\bar{\Delta}^{-1}\bar{F}\text{diag}_i(e^{p_i^*})$$

and

$$\sigma(\nabla\Phi^{out}(0)) = \sigma\left(\text{diag}_i\left(\frac{\bar{L}_i^\dagger - 1}{\bar{L}_i^\dagger}\frac{\bar{\gamma}_i^*}{\bar{\gamma}_i^* + 1}\right)\bar{\Delta}^{-1}\bar{F}\right).$$

Remark 5: The equilibrium eigenvalues of the outer loop feedback are given by a similar expression as for the inner loop.

Proof: We will use the relations

$$\frac{\bar{\sigma}_i^2}{\bar{G}^i e^{p^*}} = \frac{1 - \bar{L}_i^\dagger}{\bar{L}_i^\dagger}, \text{ and } \quad \frac{\bar{g}_{ii}e^{p_i^*}}{\bar{G}^i e^{p^*} + \bar{\sigma}_i^2} = \frac{\bar{\gamma}_i^*}{\bar{\gamma}_i^* + 1}.$$

The Jacobian can be written elementwise as

$$\nabla\Phi^{out}(0)_{ij} = \begin{cases} 0, & i = j, \\ \frac{-\bar{\sigma}_i^2\bar{g}_{ij}e^{p_j^*}}{(\bar{G}^i e^{p^*}+\bar{\sigma}_i^2)(\bar{G}^i e^{p^*})}, & i \neq j, \end{cases} = \begin{cases} 0, & i = j, \\ \frac{1}{e^{p_i^*}}\frac{\bar{L}_i^\dagger - 1}{\bar{L}_i^\dagger}\frac{\bar{g}_{ii}e^{p_i^*}}{\bar{G}^i e^{p^*}+\bar{\sigma}_i^2}\frac{\bar{g}_{ij}}{\bar{g}_{ii}}e^{p_j^*}, & i \neq j, \end{cases} = \begin{cases} 0, & i = j, \\ \frac{1}{e^{p_i^*}}\frac{\bar{L}_i^\dagger - 1}{\bar{L}_i^\dagger}\frac{\bar{\gamma}_i^*}{\bar{\gamma}_i^*+1}\frac{\bar{g}_{ij}}{\bar{g}_{ii}}e^{p_j^*}, & i \neq j. \end{cases}$$

Hence

$$\nabla\Phi^{out}(0) = \text{diag}_i\left(\frac{1}{e^{p_i^*}}\frac{\bar{L}_i^\dagger - 1}{\bar{L}_i^\dagger}\frac{\bar{\gamma}_i^*}{\bar{\gamma}_i^* + 1}\right)\bar{\Delta}^{-1}\bar{F}\text{diag}_i(e^{p_i^*}),$$

and the eigenvalue relation follows from similarity. ∎

Both $\nabla\Phi^{in}(0)$ and $\nabla\Phi^{out}(0)$ contain the matrix $\bar{\Delta}^{-1}\bar{F}$ and diagonal matrices. This makes it possible to write them as functions of each other. We have

$$\nabla\Phi^{in}(0) = \text{diag}_i\left(\frac{\bar{L}_i^\dagger}{\bar{L}_i^\dagger - 1}(\bar{\gamma}_i^* + 1)\right)\nabla\Phi^{out}(0), \tag{12}$$

$$\nabla\Phi^{out}(0) = \text{diag}_i\left(\frac{\bar{L}_i^\dagger - 1}{\bar{L}_i^\dagger}\frac{1}{\bar{\gamma}_i^* + 1}\right)\nabla\Phi^{in}(0). \tag{13}$$

For clarity of notation, denote the scaled Lipschitz constants in the equilibrium point, $z = 0$, by

$$L_D^{in}(0) := L[\hat{\Phi}^{in}; D^{-1}B^*(0)]$$
$$L_D^{out}(0) := L[\hat{\Phi}^{out}; D^{-1}B^*(0)].$$

At the equilibrium point we have

$$L_D^{in}(0) = \inf_{D\in\mathcal{D}} |D^{-1}\nabla\Phi^{in}(0)D|_1 = \rho(\nabla\Phi^{in}(0))$$
$$L_D^{out}(0) = \inf_{D\in\mathcal{D}} |D^{-1}\nabla\Phi^{out}(0)D|_1 = \rho(|\nabla\Phi^{out}(0)|)$$

where $\rho(\cdot)$ is the spectral radius and $|\cdot|$ means componentwise absolute value. By Theorem 8.4.4 in [12] it holds that if M is an elementwise positive and irreducible matrix, then $\rho(M) = \lambda_{\max}(M) > 0$ is a simple eigenvalue of M and there exists a corresponding eigenvector $x > 0$ such that $Mx = \rho(M)x$. This implies that

$$\rho(M) = \frac{1}{x_i}\sum_{j=1}^{n} M_{ij}x_j, \quad \forall i.$$

We now use this to determine the scaling multipliers. If we take $D = \text{diag}_i(x_i)$, where x is the eigenvector corresponding to $\rho(\nabla\Phi^{in})$, we get the lowest possible maximum row sum and Lipschitz constant for the inner loop. If we instead take the scalings to be the eigenvector corresponding to $\rho(\nabla\Phi^{out})$ we minimize the Lipschitz constant of the outer loop.

Given a choice of scalings to minimize one of the nonlinearities, we use the relation between $\nabla\Phi^{in}$ and $\nabla\Phi^{out}$ in (12), (13) to obtain the Lipschitz constant of the other.

We assume $\bar{G}$ to be positive to ensure that the scalings are strictly positive to avoid division by zero.

Proposition 13: Assume that $\bar{G}$ is a positive matrix. Let the scalings be equal to the eigenvector corresponding to $\rho(\nabla\Phi^{in}(0))$. Then the Lipschitz constants are given by

$$L_D^{in}(0) = \rho(\nabla\Phi^{in}(0))$$
$$L_D^{out}(0) \leq \max_i \left| \frac{\bar{L}_i^\dagger - 1}{\bar{L}_i^\dagger} \frac{1}{\bar{\gamma}_i^* + 1} \right| \rho(\nabla\Phi^{in}(0)).$$

Let the scalings be equal to the eigenvector corresponding to $\rho(|\nabla\Phi^{out}(0)|)$. Then the Lipschitz constants are given by

$$L_D^{out}(0) = \rho(|\nabla\Phi^{out}(0)|)$$
$$L_D^{in}(0) \leq \max_i \left| \frac{\bar{L}_i^\dagger}{\bar{L}_i^\dagger - 1} (\bar{\gamma}_i^* + 1) \right| \rho(|\nabla\Phi^{out}(0)|).$$

Proof: $\bar{G}$ positive implies that $\nabla\Phi^{in}(0)$ and $|\nabla\hat{\Phi}^{out}(0)|$ are positive. We have from (13) that

$$\nabla\Phi^{out}(0) = \text{diag}_i\left(\frac{\bar{L}_i^\dagger - 1}{\bar{L}_i^\dagger}\right) \text{diag}_i\left(\frac{1}{\bar{\gamma}_i^* + 1}\right) \nabla\Phi^{in}(0).$$

Let $D = \text{diag}_i(x_i)$, where x is the eigenvector corresponding to $\rho(\nabla\Phi^{in}(0))$. Since $\bar{G}$ is positive, D^{-1} is well defined. We get

$$\begin{aligned} |\nabla\hat{\Phi}^{out}(0)|_1 &= |D^{-1}\nabla\Phi_{out}(0)D|_1 \\ &= |\text{diag}_i\left(\frac{\bar{L}_i^\dagger - 1}{\bar{L}_i^\dagger} \frac{1}{\bar{\gamma}_i^* + 1}\right) D^{-1}\nabla\Phi_{in}(0)D|_1 \\ &\leq \max_i \left| \frac{\bar{L}_i^\dagger - 1}{\bar{L}_i^\dagger} \frac{1}{\bar{\gamma}_i^* + 1} \right| \rho(\nabla\Phi^{in}(0)). \end{aligned}$$

Note that we have equality if

$$\frac{\bar{L}_i^\dagger - 1}{\bar{L}_i^\dagger} \frac{1}{\bar{\gamma}_i^* + 1} = \frac{\bar{L}_j^\dagger - 1}{\bar{L}_j^\dagger} \frac{1}{\bar{\gamma}_j^* + 1}, \quad \forall (i,j).$$

The second statement is proved similarly. ■

VIII. Simulations

In this section we consider several different aspects of the joint system. First we consider pole placement in the fast inner power control loop. This is followed by a simple example where the stability conditions can be expressed explicitly in terms of the system parameters. Then we consider how the outer loop can prevent power rushes. This includes both power rushes due to aggressive feedback in the inner loop and power rushes due to infeasibility of the inner loop. We then simulate and discuss infeasibility of the joint system as defined in Definition 1. Finally we model and simulate the WCDMA system. The time-scale model in Section III-C is verified and we study how stability is effected by delays, controller gains and the target total load.

In most examples we study a typical scenario with data traffic users. In each cell there is one strong user and there is intercell interference between three cells. This implies that the interference connection between the data users is stronger and more direct, compared to voice traffic scenarios, where the interference consists of the sum over many small interfering sources.

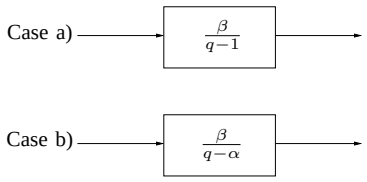

Fig. 9. Inner loop control options. a) The classical integrator control with gain β. b) Integrating control with pole placement.

A. Pole placement in the inner control loop

In this section we consider stability and performance for two cases in parallel. Case a) with an integrator in the inner loop and Case b) with a different pole placement. The inner loop control is illustrated in Figure 9. The inner controller is on either of the forms

$$\text{a)} \quad R(q) = \frac{\beta}{q-1}, \ \text{b)} \quad R(q) = \frac{\beta}{q-\alpha},$$

which results in

$$\text{a)} \quad K_1(q) = \frac{\beta}{q-1+\beta}, \ \text{b)} \quad K_1(q) = \frac{\beta}{q-\alpha+\beta}.$$

In linear scale this corresponds to the following inner power control algorithms

$$\text{a) } \bar{p}_i[t+1] = \left(\frac{\bar{\gamma}_i^\dagger}{\bar{\gamma}_i[t]}\right)^\beta \bar{p}_i[t],$$
$$\text{b) } \bar{p}_i[t+1] = \left(\frac{\bar{\gamma}_i^\dagger}{\bar{\gamma}_i[t]}\right)^\beta \bar{p}_i[t]^\alpha.$$

The pole placement in Case b) does not change the decentralized structure whatsoever. Case b) only implies that the mobile user weights its old power with α. We can drop the integrator in the inner loop in Case b), since the outer loop guarantees that we reach the target total load in equilibrium, see Proposition 1.

Let the outer loop controller be given by

$$K_2(q) = \frac{K_I}{q-1},$$

and consider stability of the joint system. Direct application of the small gain theorem is not possible, since the l_1-norm of the term $\frac{1}{q-1}$ in the outer loop system is infinite. Therefore we rewrite the system as in Figure 6 for analysis. The l_1-norms of H_1 and H_2 depend on the specific choice of parameters and can easily be computed.

For Case a) the values are typically approximately given by

$$\|H_1\|_1 \approx 2, \quad \text{and} \quad \|H_2\|_1 \approx \frac{1}{C}, \tag{14}$$

where here $C := \max_i C_i$. It is possible to establish these values as upper bounds on the gains, given that K_I, the outer loop gain, is small enough.

For Case b) however, the values of the l_1-norms are different and depend on the values of α and β. If we let

$\alpha = \beta$ we can show the following upper bounds on the l_1-norms

$$\|H_1\|_1 \leq \frac{2\beta}{\sqrt{1-\beta^2-4\beta K_I C}}$$
$$\|H_2\|_1 \leq \frac{1}{C}\frac{1}{\sqrt{1-4\beta K_I C}}.$$

This implies that we can make $\|H_1\|_1$ arbitrary low if we let $\alpha = \beta$ be sufficiently small. The value of $\|H_2\|_1$ will be approximately $1/C$ as before. This means that the effect of the inner loop to the stability criterion in Corollary 1 can be made arbitrarily small. This corresponds to a design where the inner loop tracks the reference value very fast with a low step size. Although this extreme may not be good for system design, it indicates that pole placement in the inner loop can improve stability and convergence speed of the joint system.

B. Stability for a special system

Now consider the Lipschitz constants for a special symmetric case, where

$$\bar{G} = \begin{bmatrix} 1 & l & \dots & l \\ l & 1 & \ddots & \vdots \\ \vdots & \ddots & \ddots & l \\ l & \dots & l & 1 \end{bmatrix} \quad \text{and} \quad \bar{\sigma}^2 = \begin{bmatrix} \bar{\sigma}^2 \\ \vdots \\ \bar{\sigma}^2 \end{bmatrix}.$$

Let furthermore $\bar{L}_i^\dagger = \hat{L}^\dagger, \forall i$. For simplicity we consider the equilibrium values of the Lipschitz operators. By the simple structure expressions can be simplified. In particular we use that the equilibrium powers of the users will be equal. Let

$$C_i = \frac{\bar{\sigma}_i^2 \bar{g}_{ii} e^{p_i^*}}{(\bar{G}^i e^{p^*} + \bar{\sigma}_i^2)(\bar{G}^i e^{p^*})} = \frac{\bar{\sigma}^2 \bar{p}_i^*}{(\bar{p}_i^* + (n-1)l\bar{p}_i^* + \bar{\sigma}^2)(\bar{p}_i^* + (n-1)l\bar{p}_i^*)}.$$

We have

$$L_D^{in}(0) = \frac{\bar{F}^i \bar{p}^*}{\bar{F}^i \bar{p}^* + \bar{\sigma}_i^2} = \frac{(n-1)l\bar{p}_i^*}{(n-1)l\bar{p}_i^* + \bar{\sigma}^2} = (n-1)l\bar{\gamma}^*,$$

and

$$L_D^{out}(0) = \frac{\bar{\sigma}_i^2 \bar{F}^i \bar{p}^*}{(\bar{G}^i e^{p^*} + \bar{\sigma}_i^2)(\bar{G}^i e^{p^*})} = \frac{\bar{\sigma}^2 (n-1) l \bar{p}_i^*}{(\bar{p}_i^* + (n-1)l\bar{p}_i^* + \bar{\sigma}^2)(\bar{p}_i^* + (n-1)l\bar{p}_i^*)}.$$

Now consider the stability criterion in Corollary 1 for Case a) and b) studied in the previous section. For Case a) the stability criterion is then approximately

$$\begin{aligned} &\|H_1\|_1 L_D^{in}(0) + \|H_2\|_1 L_D^{out}(0) \\ &\approx 2L_D^{in}(0) + \frac{1}{C} L_D^{out}(0) \\ &= 2(n-1)l\bar{\gamma}^* \\ &\quad + \frac{1}{C}\frac{\bar{\sigma}^2 (n-1) l \bar{p}_i^*}{(\bar{p}_i^* + (n-1)l\bar{p}_i^* + \bar{\sigma}^2)(\bar{p}_i^* + (n-1)l\bar{p}_i^*)} \\ &= 2(n-1)l\bar{\gamma}^* + (n-1)l \\ &< 1. \end{aligned}$$

From this we get the following condition on the size of the cross-coupling gains

$$l < \frac{1}{(2\bar{\gamma}^* + 1)(n-1)},$$

or the following condition on the equilibrium SIR

$$\bar{\gamma}^* < \frac{1-(n-1)l}{2(n-1)l}. \tag{15}$$

For Case b) we can obtain $\|H_1\|_1 L_D^{in}(0) < \epsilon$, by letting $\alpha = \beta$ be sufficiently small. A similar stability analysis as above gives the following condition on the size of the cross-coupling gains

$$l < \frac{1-\epsilon}{n-1}.$$

Consider a numeric example with $l = 0.1$, $\bar{\sigma}^2 = 0.05$ and the total load target equal for all users. For Case a) we get the approximate bound $\bar{\gamma}^* < 2$, by (15). This corresponds to the total load target 0.8. Stability can hence be guaranteed for $\bar{L}_i^\dagger = \hat{L}^\dagger < 0.8, \forall i$. A simulation for the system in Case a) with $\beta = 0.9$ and $K_I = 0.5$ is shown in Figure 10. The system is disturbed from the equilibrium by a pulse in the transmission powers. The system shows good stability properties. The computed l_1-norms are in this case $\|H_1\|_1 \approx 1.98$ and $\|H_2\|_1 \approx C$, which shows that the l_1-norm-approximation is valid.

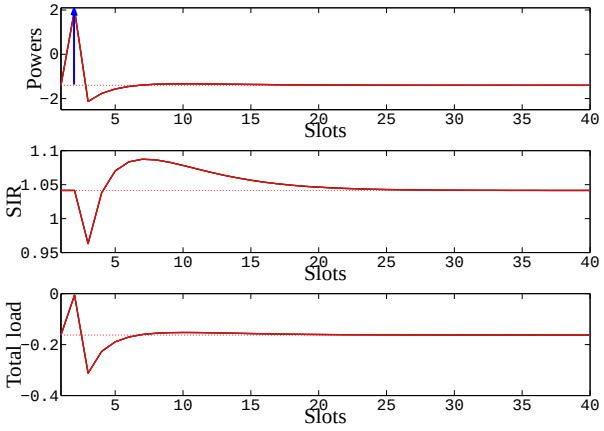

Fig. 10. Simulation of a simple example. The system is stable for the choice of $\beta = 0.9$ and $K_I = 0.5$ when subject to an impulse disturbance. Note that the powers, SIR and total load are in logarithmic scale.

C. Prevention of power rushes

In this section we show how power rushes can be prevented by using an outer control loop. Let

$$\bar{G} = \begin{bmatrix} 1 & 0.001 & 0.005 \\ 0.025 & 1 & 0.0025 \\ 0.01 & 0.001 & 1 \end{bmatrix}, \quad \bar{\sigma}^2 = \begin{bmatrix} 0.05 \\ 0.05 \\ 0.05 \end{bmatrix}.$$

Note that the system parameters are the same as in the example in Section V, where the QoS was shown as a function of the total load. Here we use the total load target

$$\tilde{L}^\dagger = \begin{bmatrix} 0.8 & 0 & 0 \\ 0 & 0.8 & 0 \\ 0 & 0 & 0.8 \end{bmatrix},$$

which corresponds to the equilibrium powers, $\bar{p}^*$, and equilibrium SIRs, $\bar{\Gamma}^*$,

$$\bar{p}^* = \begin{bmatrix} 0.1988 \\ 0.1945 \\ 0.1978 \end{bmatrix}, \quad \bar{\Gamma}^* = \begin{bmatrix} 3.8844 & 0 & 0 \\ 0 & 3.5074 & 0 \\ 0 & 0 & 3.7909 \end{bmatrix}.$$

We consider two causes for power rushes in the inner loop. From e.g. [17] and [18] we know that a too high controller gain together with a delay can make the system unstable. Another reason for power rushes is when the target SIR is set too high and the users start competing using increasing powers. This problem is avoided in most literature by only considering feasible systems, which means that these cases are not considered.

1) Delay and high gain: Consider first the case with delay together with high gain. Let the controllers be given by

$$R(q) = \frac{\beta}{q(q-1)}, \quad K_2(q) = \frac{K_I}{q-1},$$

where $\beta = 0.8$ and $K_I = 0.1$ for all users and there is a delay in the inner loop.

First consider the inner loop separately with constant reference value. The simulation in Figure 11 shows that, although the system is feasible, a power rush is caused by the single delay in combination with the relatively high value of β.

Now consider stability of the joint system with use of Corollary 1.

$$\begin{aligned} &\|H_1\|_1 L_D^{in}(0) + \|H_2\|_1 L_D^{out}(0) \\ &= 6.6302 * 0.0364 + 5.0298 * 0.0020 \\ &= 0.2513 < 1. \end{aligned}$$

A simulation of the joint system can be seen in Figure 12. The joint dynamics are stable and converge to the equilibrium point. For this example we can show local stability for common total load targets up to around 0.95.

2) Infeasible inner loop: Now consider the second case with an infeasible inner loop system. Let the controllers be given by

$$R(q) = \frac{\beta}{q-1}, \quad K_2(q) = \frac{K_I}{q-1}, \tag{16}$$

where $\beta = 0.7$ and $K_I = 0.1$ for all users.

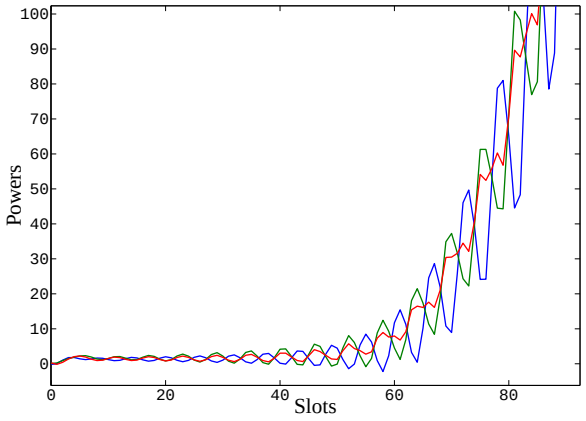

Fig. 11. A power rush is caused by a single delay in the inner loop together with too aggressive feedback. The powers are in logarithmic scale.

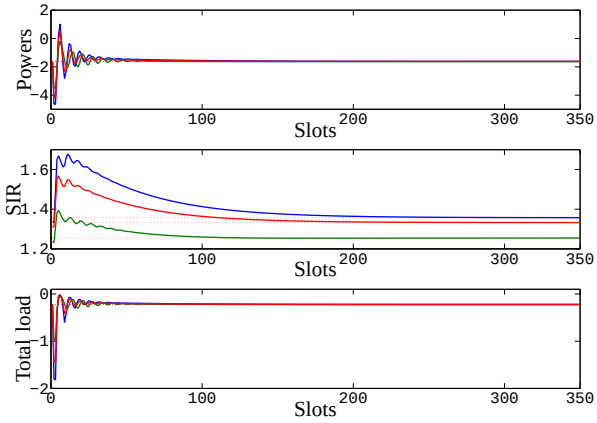

Fig. 12. Simulation where the inner loop by itself would cause a power rush, but the joint system is stabilized by the outer control algorithm. Note that the powers, SIR and total load are in logarithmic scale.

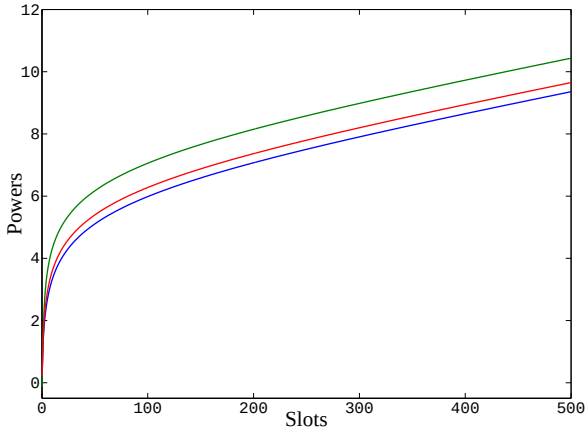

Fig. 13. Power rush caused by infeasible inner loop system. The SIR-target is set higher than any reachable SIR, which makes the users compete with increasing transmission powers. The powers are in logarithmic scale.

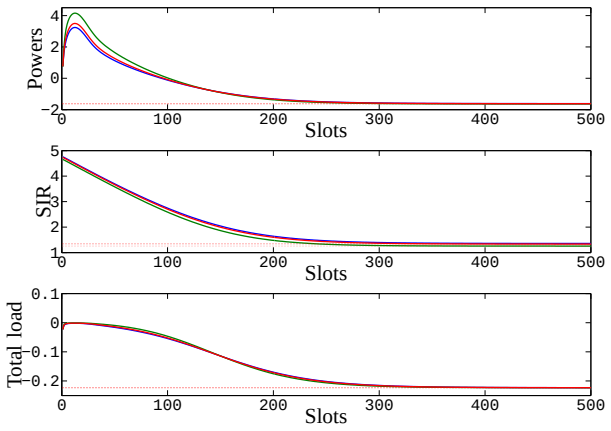

Fig. 14. This figure illustrates how the outer loop can prevent a power rush and stabilize the system. Initially the SIR-target is set too high and the powers start to increase, just as in Figure 13. However, the experienced total load is above the total load target, so the outer control loop decreases the SIR-target, stabilizing the system. The simulation starts in equilibrium and in time zero a step in the SIR is applied. Note that the powers, SIR and total load are in logarithmic scale.

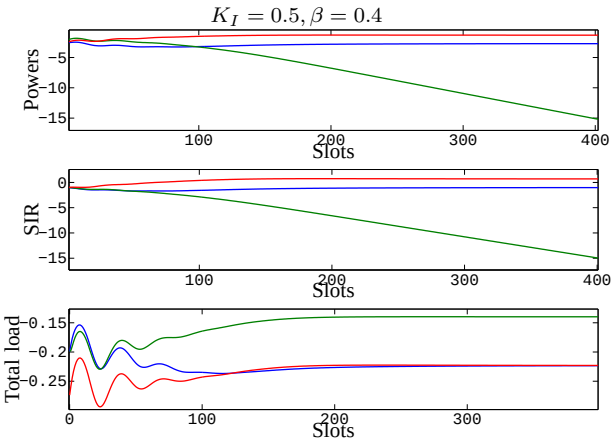

Fig. 15. Joint inner and outer loop simulation for an infeasible case. User two leaves the system. The controllers are given in (16) with $\beta = 0.4$ and $K_I = 0.5$. Note that the powers, SIR and total load are in logarithmic scale.

The maximal common feasible SIR-target of the inner loop is given by the limit $\frac{1}{\rho(\Delta^{-1}F)} \approx 104$, i.e. $\gamma_i^\dagger \approx 4.64$ in logarithmic scale. Figure 13 shows the inner power control loop separated with the constant SIR-target value $\gamma_i^\dagger = 4.65, \forall i$. The transmission powers of the users tend to infinity. When applying the outer loop control to the system, initialized with a SIR-target of about 4.7 in logarithmic scale, the system is stabilized, see Figure 14.

The controllers used in this example corresponds to Case a) studied in Section VIII-A. We use the approximate values of the gains in (14) and compute the equilibrium Lipschitz constants with use of Proposition 11 and 13. We get that $L_D^{in}(0) = 0.0364$, $L_D^{out}(0) = 0.0444$ and $C = 0.1988$. The stability condition is fulfilled since

$$\begin{aligned} &\|H_1\|_1 L_D^{in}(0) + \|H_2\|_1 L_D^{out}(0) \\ &= 1.9331 * 0.0364 + 5.0298 * 0.0020 \\ &= 0.0805 < 1. \end{aligned}$$

For this example we can show local stability for a common total load target up to around 0.99.

D. System infeasibility

An important issue in cellular networks is the robustness in the system to introduce new users and changes in the system parameters. If the changes are too large, the system may become infeasible. This corresponds to that the experienced total load is higher than the target total load for at least one user. Dynamically this implies that the base station of an affected user decreases the target SIR, which typically leads to lower transmission powers. Since no positive powers exist, such that the experienced total load is equal to the target total load, this drives the transmission powers of the user to zero, i.e. the user leaves the system. This is a desirable behaviour that makes the system self-regulating, in contrast to the unstable behaviour of an infeasible inner power control loop. This is related to the problem of active link protection studied in e.g. [2].

Which user or users that will leave the system is not obvious due to the dynamic behaviour of the system and it depends on the initial states. To see this, consider the infeasible example with

$$\bar{G} = \begin{bmatrix} 1 & 1 & 0.5 \\ 1 & 0.5 & 1 \\ 0.5 & 0.625 & 0.625 \end{bmatrix}, \quad \bar{\sigma}^2 = \begin{bmatrix} 0.05 \\ 0.05 \\ 0.05 \end{bmatrix}$$

and where $\tilde{L}^\dagger = \text{diag}_i(0.8)$. Let the controllers be as in (16), but with $\beta = 0.4$ and $K_I = 0.5$ for all users. An example with the same parameter values was also studied in Section V. The equilibrium power vector is $\bar{p}^* = [-0.1,\ 0.2,\ 0.2]^T$, which corresponds to the equilibrium SIRs $\bar{\gamma}^* = [-0.2857, 0.6667, 1]^T$. A simulation of the joint system is shown in Figure 15. The transmission power of the second user goes to zero. The total load of all the users is stabilized, but for the second user it is too high, which implies that the target SIR is continuously decreased. This outcome may seem reasonable since the second row of the G-matrix has the largest off-diagonal elements. However, the infeasible equilibrium point suggests that the first user would get negative powers, so another guess could be that the powers of user one would go to zero.

Repeating the simulation with different values on the initial conditions and different controller gains, another outcome is obtained. The powers of both user one and three go to zero, and only user two remains active, see Figure 16. This suggests that it is non-trivial to predict the final allocations.

E. WCDMA modelling

In this section we model the WCDMA system with time-scale difference and delays. We use the same example to

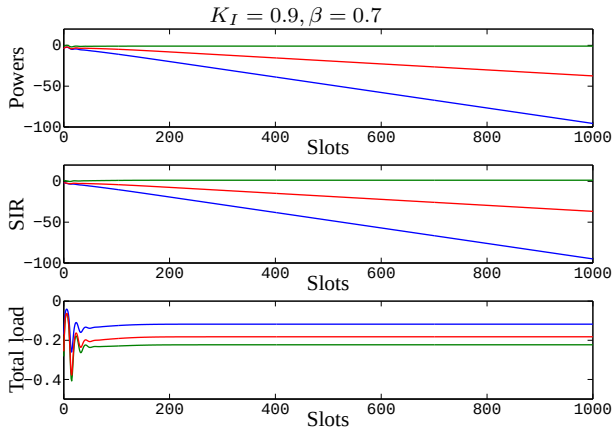

Fig. 16. Joint inner and outer loop simulation for an infeasible case. User one and three leaves the system. The controllers are given in (16) with $\beta = 0.7$ and $K_I = 0.9$. Note that the powers, SIR and total load are in logarithmic scale.

validate the model derived in Section III and to study how stability and performance is affected by the choice of controller gains, delays and the choice of total load target.

The WCDMA system typically has a time-scale difference of 15 slots and an additional delay of $d = 15$ slots. We use the outer loop controller $K_0(q) = \frac{K_I}{q-1}$ and this corresponds to the outer loop transfer function

$$\begin{aligned} K_2(q) &= q^{-d}\hat{K}_0(q^{15})\hat{L}(q)\left(\frac{1-q^{-15}}{1-q^{-1}}\right) \\ &= q^{-15}\frac{K_I}{q^{15}-1}\hat{L}(q)\left(\frac{1-q^{-15}}{1-q^{-1}}\right) \\ &= \frac{K_I}{q^{29}(q-1)}\hat{L}(q), \end{aligned}$$

where the cut-off frequency of the low-pass filter should be given by $w_s = \frac{\pi}{15}$.

The inner power control loop typically has a delay of two. This renders the inner loop transfer function

$$R(q) = \frac{\beta}{q^2(q-1)}.$$

Let the system parameters be given by

$$\bar{G} = \begin{bmatrix} 1 & 0.001 & 0.005 \\ 0.025 & 1 & 0.0025 \\ 0.01 & 0.001 & 1 \end{bmatrix},$$

$$\bar{\sigma}^2 = \begin{bmatrix} 0.05 \\ 0.05 \\ 0.05 \end{bmatrix} \quad \text{and} \quad \tilde{L}^\dagger = \begin{bmatrix} 0.8 & 0 & 0 \\ 0 & 0.8 & 0 \\ 0 & 0 & 0.8 \end{bmatrix}.$$

This corresponds to the equilibrium powers, $\bar{p}^*$, and equilibrium SIRs, $\bar{\Gamma}^*$,

$$\bar{p}^* = \begin{bmatrix} 0.1988 \\ 0.1945 \\ 0.1978 \end{bmatrix}, \quad \bar{\Gamma}^* = \begin{bmatrix} 3.8844 & 0 & 0 \\ 0 & 3.5074 & 0 \\ 0 & 0 & 3.7909 \end{bmatrix}.$$

Let $\beta = 0.5$ and $K_I = 0.05$ and assume we are using the simple low-pass filter $L(q) = \frac{0.75}{(q-0.5)(q+0.5)}$.

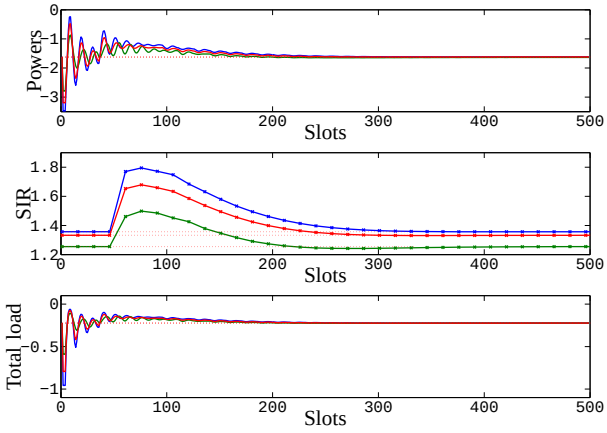

Fig. 17. WCDMA system with use of Simulink blocks for down- and upsampling as indicated in Figure 4. We can see that the SIR is updated only every 15:th time step. The time-scale difference between the inner and outer loop is set to 15 and an additional delay of 15 is modelled in the outer loop. The inner loop is modelled with a delay of 2. Note that the powers, SIR and total load are in logarithmic scale.

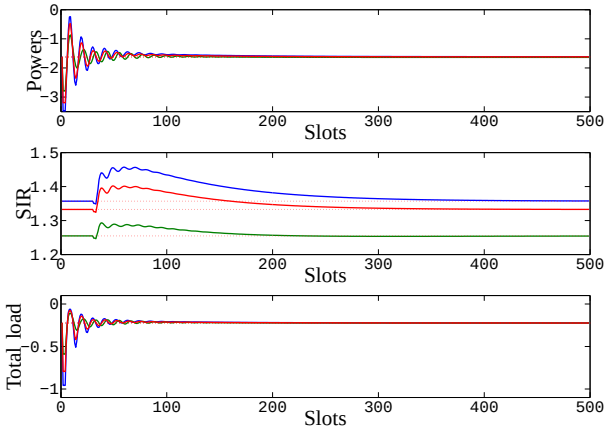

Fig. 18. The same WCDMA system as simulated in Figure 17, but with the derived time-scale model in the outer loop controller. The approximation is good, although a low order low-pass filter is used. Stability can be guaranteed by Corollary 1. Note that the powers, SIR and total load are in logarithmic scale.

1) Time-scale modelling: First consider a simulation using a Simulink model with designated blocks for downsampling and upsampling by zero order hold. This is shown in Figure 17. Then consider the same simulation with the time-scale model from Section III in Figure 18. The derivation of the transfer function is based on the assumption of an ideal low-pass filter, and in this example only a low order filter was used. Still the dynamics of the models are quite similar, which justifies analysis on the simplified model.

2) Stability and controller parameters: Now consider stability. In the equilibrium point the joint system gain is

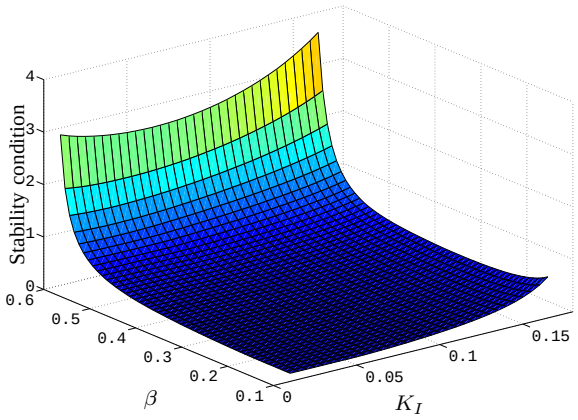

Fig. 19. The joint system gain for the WCDMA example as a function of the controller gains β and K_I. Stability of the system can be guaranteed for all combinations giving a value less than 1.

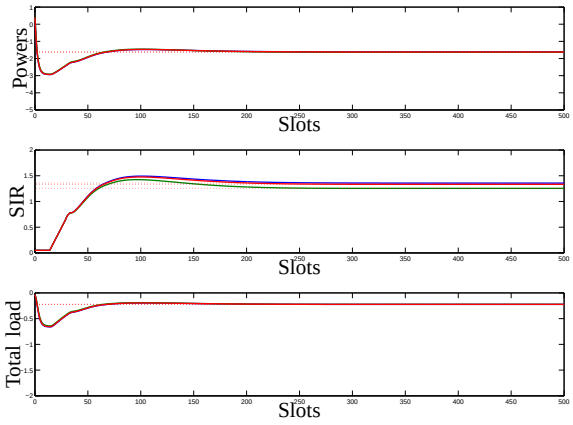

Fig. 20. Joint system simulation for the WCDMA example with no delay in the inner loop. Note that the powers, SIR and total load are in logarithmic scale.

given by

$$\|H_1\|_1 L_D^{in}(0) + \|H_2\|_1 L_D^{out}(0)$$
$$= 12.6 * 0.0364 + 5.03 * 0.0020 = 0.4694 < 1,$$

so by Corollary 1 we expect the system to be stable in a neighbourhood around the equilibrium point. This was already verified by the simulation in Figure 18.

For design it is interesting how the joint system gain depends on the design parameters β and K_I. In Figure 19 the joint system gain is shown for varying β and K_I. Local stability is guaranteed for all values below one.

3) Stability and delay: System performance heavily depend on the size of the delays in the system. In Figure 20, 21 and 22 we consider the cases where the inner loop has zero, one and two delays respectively. Higher delay in the inner loop together with a higher inner loop gain gives an oscillatory behaviour with a relatively high frequency. Stability of the joint system can easily be affected, for example if the outer loop is too slow to prevent a power rush. To some extent the choice of outer loop gain can improve the performance, but it cannot remove the oscillatory behaviour completely. An example is shown in Figure 23, where the inner loop has one delay and a high gain. In this case, stability can still be achieved using a very low outer loop gain. Setting a low outer loop gain typically makes the system more robust, but to the cost of a slower convergence rate.

If the inner loop has no delay and an appropriate value of the gain, it will track the reference value of the outer loop without difficulty. However, since the outer loop also is delayed, a too high outer loop gain can also lead to instability. This is shown in Figure 24.

4) Stability and total load: Another design parameter is the target total load. In Figure 25 we can see the Lipschitz constants of the outer and inner loop in equilibrium as functions of the total load target, $\bar{L}_i^{\dagger} = \hat{L}^{\dagger}, i = 1, 2, 3$. Two values are plotted for each Lipschitz constant. The solid line

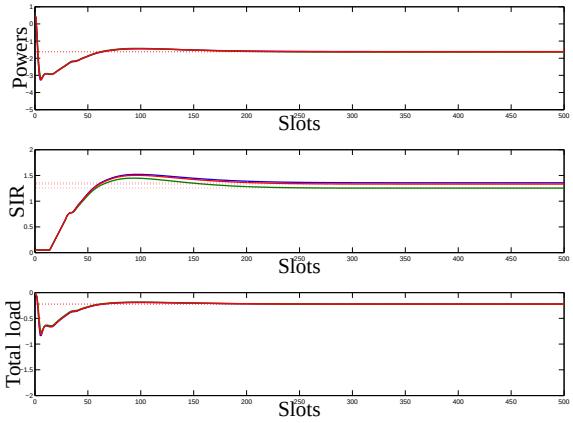

Fig. 21. Joint system simulation for the WCDMA example with one delay in the inner loop. Note that the powers, SIR and total load are in logarithmic scale.

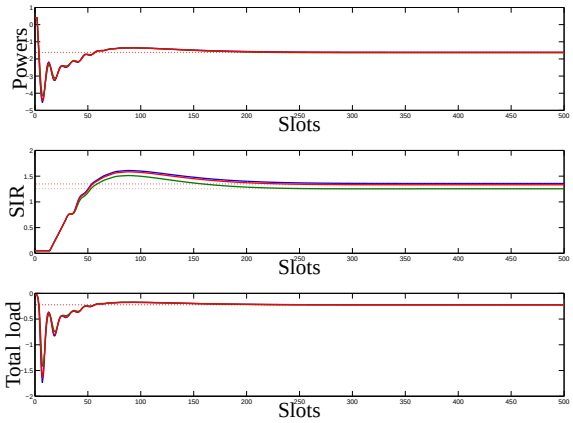

Fig. 22. Joint system simulation for the WCDMA example with two delays in the inner loop. Note that the powers, SIR and total load are in logarithmic scale.

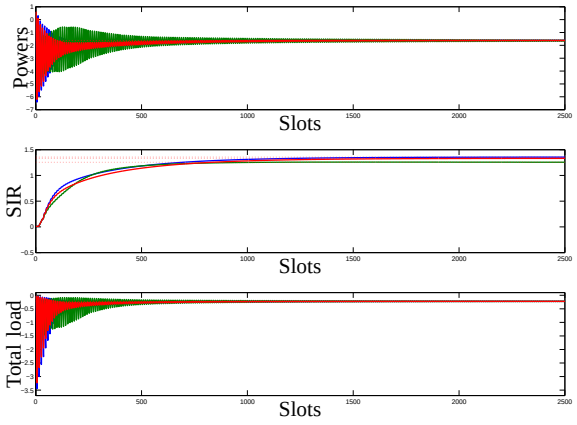

Fig. 23. Joint system simulation for the WCDMA example where the inner loop is delayed and has a high gain. The system is stabilized by using a low gain in the outer loop controller. Note that the powers, SIR and total load are in logarithmic scale.

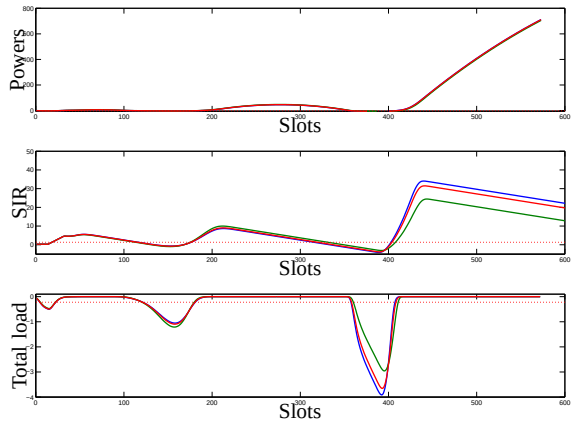

Fig. 24. A simulation for the WCDMA example where a high gain in the outer loop controller causes instability of the joint system. Note that the powers, SIR and total load are in logarithmic scale.

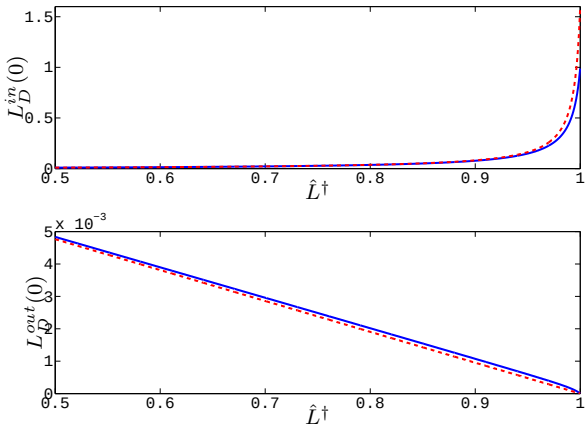

Fig. 25. Lipschitz constants as functions of the total load target. All users are given the same total load target and the constant C is chosen as in (11). The solid line is for the case when the scaling multipliers are chosen with respect to the inner loop nonlinearity, and the dashed line when chosen with respect to the outer loop nonlinearity. As expected, the Lipschitz constants are lower in the case when they are optimized on.

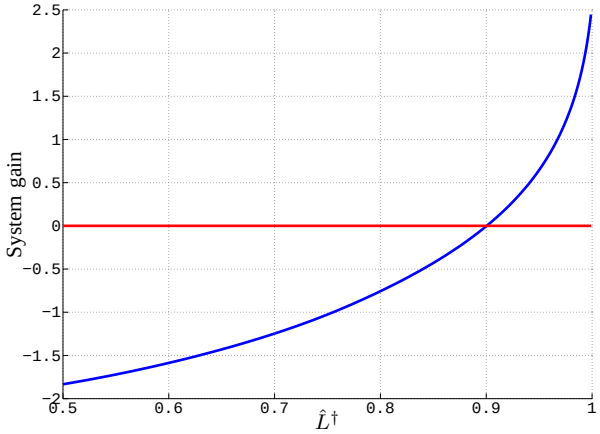

Fig. 26. Joint system gain in the equilibrium. Stability can be guaranteed by Corollary 1 when below zero. For this example stability can be guaranteed for $\hat{L}^\dagger \leq 0.9$.

represents when the optimization of the scaling multipliers is done with respect to the inner loop and the dashed line when it is done with respect to the outer loop. The Lipschitz constants have a fundamentally different behaviour. The inner loop Lipschitz constant is large when $\hat{L}^\dagger$ is close to one and is then critical for system stability. The outer loop Lipschitz constant, on the other hand, decreases almost linearly with increasing $\hat{L}^\dagger$. We make the conclusion that to prove stability for higher values of the total load target, it is a good choice to optimize the scalings over the inner loop Lipschitz constant. In [18] and [19] the problem of optimizing scaling multipliers for the inner loop was studied in detail.

Finally consider the joint system gain in the equilibrium as a function of the total load target. We use the choice of C given in (11), which makes the relation highly non-linear. From Proposition 2 we have that $\bar{L}^\dagger$ determines the equilibrium point, which effects both $L_D^{in}(0)$ and $L_D^{out}(0)$. This was also seen in Figure 25. Furthermore, our choice of the constant C is dependent on the equilibrium point, so also $\|H_1\|_1$ and $\|H_2\|_1$ are affected. In Figure 26 the joint system gain is plotted in logarithmic scale as a function of the target total load. For this example and method, the highest total load target for which stability can be guaranteed is around 0.9. The joint system gain in the equilibrium is, as indicated in Figure 19, also dependent on the choice of β and K_I. For other combinations of them, system stability can be guaranteed for significantly higher values of $\hat{L}^\dagger$.

IX. Conclusions

In this paper we introduce a framework that can be used to model rate and power control in a cellular network. It is based on distributed high order algorithms that use locally measurable data for feedback. Modelling of filters, delays and time-scale differences is straightforward to include. We perform stability analysis of the nonlinear system and give sufficient conditions for stability. The results are sharpened and structure of the problem revealed.

Simulations and examples show that the model has desirable stabilizing properties.

References

[1] M. Abbas-Turki, F. de S. Chaves, H. Abou-Kandil, and J. M. T. Romano. Mixed h2/h power control with adaptive qos for wireless communication networks. In *Proc. of the 10th European Control Conference (ECC'09)*, Budapest, Hungary, 2009.

[2] N. Bambos, S.C. Chen, and G.J. Pottie. Channel access algorithms with active link protection for wireless communication networks with power control. *Networking, IEEE/ACM Transactions on*, 8(5):583 – 597, October 2000.

[3] T. Charalambous and Yassine Ariba. On the stability of a power control algorithm for wireless networks in the presence of time-varying delays. In *Proceedings of the European Control Conference*, Budapest, Hungary, 2009.

[4] T. Charalambous, I. Lestas, and G. Vinnicombe. On the stability of the Foschini-Miljanic algorithm with time-delays. In *Proceedings of the 47th IEEE Conference on Decision and Control*, Cancun, Mexico, 2008.

[5] M. Chiang, P. Hande, T. Lan, and C.W. Tan. Power control in wireless cellular networks. *Foundations and Trends in Communications and Information Theory*, 2(4):1–156, 2008.

[6] Mung Chiang and J. Bell. Balancing supply and demand of bandwidth in wireless cellular networks: utility maximization over powers and rates. In *INFOCOM 2004. Twenty-third AnnualJoint Conference of the IEEE Computer and Communications Societies*, volume 4, pages 2800 – 2811 vol.4, 2004.

[7] M.A. Dahleh and I. Diaz-Bobillo. *Control of Uncertain Systems: A Linear Programming Approach*. Prentice-Hall, 1995.

[8] G. J. Foschini and Z. Miljanic. Distributed autonomous wireless channel assignment algorithm with power control. *IEEE Transactions on Vehicular Technology*, 44(3):420–429, 1995.

[9] Erik Geijer Lundin. *Uplink Load in CDMA Cellular Radio Systems*. Linkping studies in science and technology. dissertations no 977, November 2005.

[10] F. Gunnarsson. *Power Control in Cellular Radio Systems: Analysis, Design and Estimation*. PhD thesis, Linköping University, Linköping, Sweden, 2000.

[11] F. Gunnarsson and F. Gustafsson. Control theory aspects of power control in UMTS. *Control Engineering Practice*, 11(10):1113–1125, 2003.

[12] Roger A. Horn and Charles R. Johnson. *Matrix Analysis*. Cambridge University Press, 1990.

[13] S.A. Jafar and A. Goldsmith. Adaptive multirate cdma for uplink throughput maximization. *Wireless Communications, IEEE Transactions on*, 2(2):218 – 228, March 2003.

[14] S. Kandukuri and S. Boyd. Simultaneous rate and power control in multirate multimedia cdma systems. In *Spread Spectrum Techniques and Applications, 2000 IEEE Sixth International Symposium on*, 2000.

[15] E. Geijer Lundin and F. Gunnarsson. Uplink load in cdma cellular radio systems. *IEEE Transactions on Vehicular Technology*, 55(4):1331 – 1346, 2006.

[16] A. Möller and U. T. Jönsson. Stability of high order distributed power control. In *Proceedings of the 48th IEEE Conference on Decision and Control*, Shanghai, China, 2009.

[17] A. Möller and U. T. Jönsson. Stability of systems under interference feedback. In *Proceedings of the European Control Conference*, Budapest, Hungary, 2009.

[18] A. Möller and U. T. Jönsson. Input output analysis of power control in wireless networks. In *Proceedings of the 49th IEEE Conference on Decision and Control*, Atlanta, USA, 2010.

[19] A. Möller and U. T. Jönsson. Input output analysis of power control in wireless networks. Technical Report TRITA-MAT-10-OS03, Dept. of Mathematics, Royal Inst. of Technology, September 2010. A short version appeared in Proceedings of the 49th IEEE Conference on Decision and Control.

[20] Subramanian and A.H. A.; Sayed. Joint rate and power control algorithms for wireless networks. *IEEE Transactions on Signal Processing*, 53(11):4204–4214, 2005.

[21] C. W. Sung and K.-K. Leung. A generalized framework for distributed power control in wireless networks. *IEEE Transactions on Information Theory*, 51(7):2625–2635, 2005.

[22] Mingbo Xiao, N.B. Shroff, and E.K.P. Chong. A utility-based power-control scheme in wireless cellular systems. *Networking, IEEE/ACM Transactions on*, 11(2):210 – 221, April 2003.

[23] R.D. Yates. A framework for uplink power control in cellular radio systems. *IEEE Journal on selected areas in communications*, 13(7):1341–1347, 1995.

Appendix

A. Proof of Proposition 1

Proof: The inner loop is given in (5) as

$$p_i[t] = K_{i,1}(q)\Big(\gamma_i^\dagger[t] - g_{ii} + \ln\Big(\sum_{j\neq i}\bar{g}_{ij}\bar{p}_j[t] + \bar{\sigma}_i^2\Big)\Big),$$

where

$$\gamma_i^\dagger[t] = K_{i,2}(q)(L_i^\dagger - L_i^{tot}[t]).$$

Define $I_i(p) := \ln\Big(\sum_{j\neq i}\bar{g}_{ij}\bar{p}_j[t] + \bar{\sigma}_i^2\Big)$. For each i we can hence write

$$\begin{aligned}
&p_i[t] = K_{i,1}(q)\Big(K_{i,2}(q)(L_i^\dagger - L_{i,tot}[t]) - g_{ii} + I_i(p)\Big) && \Leftrightarrow\\
&p_i[t] = K_{i,1}(q)K_{i,2}(q)\Big(L_i^\dagger - L_i^{tot}[t] + C_i p_i[t]\Big)\\
&\qquad - K_{i,1}(q)K_{i,2}(q)C_i p_i[t] + K_{i,1}(q)\Big(-g_{ii} + I_i(p)\Big) && \Leftrightarrow\\
&(1 + K_{i,1}(q)K_{i,2}(q)C_i)p_i[t] =\\
&\qquad K_{i,1}(q)K_{i,2}(q)\Big(L_i^\dagger - L_i^{tot}[t] + C_i p_i[t]\Big)\\
&\qquad + K_{i,1}(q)\Big(-g_{ii} + I_i(p)\Big) && \Leftrightarrow\\
&p_i[t] = \frac{K_{i,1}(q)K_{i,2}(q)}{1 + K_{i,1}(q)K_{i,2}(q)C_i}(L_i^\dagger - L_i^{tot}[t] + C_i p_i[t])\\
&\qquad + \frac{K_{i,1}(q)}{1 + K_{i,1}(q)K_{i,2}(q)C_i}(-g_{ii} + I_i(p)),
\end{aligned}$$

where C_i is a constant. Let p_i^* denote the steady state power of user i as $q \to 1$. Since the outer loop controller has an integrator, we then have

$$\begin{aligned}
&\lim_{q\to 1}\frac{K_{i,1}(q)K_{i,2}(q)}{1 + K_{i,1}(q)K_{i,2}(q)C_i} = \frac{1}{C_i}, \quad \text{and}\\
&\lim_{q\to 1}\frac{K_{i,1}(q)}{1 + K_{i,1}(q)K_{i,2}(q)C_i} = 0,
\end{aligned}$$

and hence

$$\begin{aligned}
&p_i^* = \frac{1}{C_i}(L_i^\dagger - L_i^{tot} + C_i p_i^*), \quad \forall i && \Leftrightarrow\\
&L_i^\dagger = L_i^{tot}, \quad \forall i.
\end{aligned}$$

■

B. Proof of Proposition 3

Proof: Assume first that $\rho(\bar{\Gamma}^*\bar{\Delta}^{-1}\bar{F}) < 1$. By letting the expression for SIR in (2) be equal to $\bar{\Gamma}^*$ we obtain the following expression of the equilibrium powers

$$\bar{p}^* = (I - \bar{\Gamma}^*\bar{\Delta}^{-1}\bar{F})^{-1}\bar{\Gamma}^*\bar{\Delta}^{-1}\bar{\sigma}^2.$$

Since $\bar{\Gamma}^*\bar{\Delta}^{-1}\bar{F}$ is elementwise non-negative and, under the condition $\rho(\bar{\Gamma}^*\bar{\Delta}^{-1}\bar{F}) < 1$, the inverse expression can be written as the convergent, infinite sum $\sum_{i=0}^{\infty}(\bar{\Gamma}^*\bar{\Delta}^{-1}\bar{F})^i$ of non-negative terms. Since furthermore the elements of $\bar{\Gamma}^*$ and $\bar{\Delta}^{-1}$ are non-negative and $\bar{\sigma}^2$ is positive, the powers are non-negative.

Now consider

$$\bar{p}^* = ((I - \tilde{L}^\dagger)\bar{G})^{-1}\tilde{L}^\dagger\bar{\sigma}^2 \geq 0.$$

Since $\bar{G}$ is a non-negative matrix we can equivalently write

$$\bar{G}\bar{p}^* = (I - \tilde{L}^\dagger)^{-1}\tilde{L}^\dagger\bar{\sigma}^2 \geq 0,$$

or

$$(\bar{G}\bar{p}^*)_i = \frac{\bar{L}_i^\dagger\bar{\sigma}_i^2}{1 - \bar{L}_i^\dagger} \geq 0,$$

which implies that $\bar{L}_i^\dagger \in [0, 1), \forall i$. ■

C. Proof of Proposition 4

Proof: Consider the powers

$$\bar{p}^* = ((I - \tilde{L}^\dagger)\bar{G})^{-1}\tilde{L}^\dagger\bar{\sigma}^2,$$

or equivalently

$$\bar{G}\bar{p}^* = (I - \tilde{L}^\dagger)^{-1}\tilde{L}^\dagger\bar{\sigma}^2.$$

$\bar{L}_i^\dagger \in [0, 1), \forall i$, guarantees that $\bar{G}\bar{p}^* \geq 0$. Assume that at least one element, $\bar{p}_k^*$, of $\bar{p}^*$ is negative. Then

$$\begin{aligned} \bar{\gamma}_k^* = \frac{\bar{g}_{kk}\bar{p}_k^*}{\sum_{j\neq k}\bar{g}_{kj}\bar{p}_j^* + \bar{\sigma}_k^2} \quad &\Leftrightarrow \\ \bar{\gamma}_k^*\Big(\sum_{j\neq k}\bar{g}_{kj}\bar{p}_j^* + \bar{\sigma}_k^2\Big) = \bar{g}_{kk}\bar{p}_k^*. \end{aligned}$$

Since $\bar{G}\bar{p}^* \geq 0$ and $\bar{\sigma}_k^2 > 0$, we have that

$$\Big(\sum_{j\neq k}\bar{g}_{kj}\bar{p}_j^* + \bar{\sigma}_k^2\Big) > 0,$$

and by assumption $\bar{g}_{kk}\bar{p}_k^* < 0$. This implies that $\bar{\gamma}_k^* < 0$. ■

D. Proof of Proposition 5

Proof: We have that

$$\begin{aligned} \bar{L}_i^{tot} &= \frac{\sum_{j=1}^n \bar{g}_{ij}\bar{p}_j}{\sum_{j=1}^n \bar{g}_{ij}\bar{p}_j + \bar{\sigma}_i^2} \\ &= \frac{\bar{g}_{ii}\bar{p}_i + \sum_{j\neq i}\bar{g}_{ij}\bar{p}_j}{\bar{g}_{ii}\bar{p}_i + \sum_{j\neq i}\bar{g}_{ij}\bar{p}_j + \bar{\sigma}_i^2} \\ &= \frac{\frac{\bar{g}_{ii}\bar{p}_i}{\sum_{j\neq i}\bar{g}_{ij}\bar{p}_j + \bar{\sigma}_i^2} + \frac{\sum_{j\neq i}\bar{g}_{ij}\bar{p}_j}{\sum_{j\neq i}\bar{g}_{ij}\bar{p}_j + \bar{\sigma}_i^2}}{\frac{\bar{g}_{ii}\bar{p}_i}{\sum_{j\neq i}\bar{g}_{ij}\bar{p}_j + \bar{\sigma}_i^2} + 1} \\ &= \frac{\bar{\gamma}_i + \frac{\sum_{j\neq i}\bar{g}_{ij}\bar{p}_j}{\sum_{j\neq i}\bar{g}_{ij}\bar{p}_j + \bar{\sigma}_i^2}}{\bar{\gamma}_i + 1} \\ &= \frac{\bar{\gamma}_i + \bar{K}_i}{\bar{\gamma}_i + 1}. \end{aligned}$$

Similarly we have that

$$\begin{aligned} \bar{L}_i^{tot} = \frac{\bar{\gamma}_i + \bar{K}_i}{\bar{\gamma}_i + 1} \quad &\Leftrightarrow \\ (1 + \bar{\gamma}_i)\bar{L}_i^{tot} = \bar{\gamma}_i + \bar{K}_i \quad &\Leftrightarrow \\ (1 - \bar{L}_i^{tot})\bar{\gamma}_i = \bar{L}_i^{tot} - \bar{K}_i \quad &\Leftrightarrow \\ \bar{\gamma}_i = \frac{\bar{L}_i^{tot} - \bar{K}_i}{1 - \bar{L}_i^{tot}}. \end{aligned}$$

■

E. Proof of Proposition 6

Proof: Under the assumption that $\rho(\bar{\Gamma}^*\bar{\Delta}^{-1}\bar{F}) < 1$, the following equation gives the power as a function of the SIR

$$\bar{p} = (I - \bar{\Gamma}^*\bar{\Delta}^{-1}\bar{F})^{-1}\bar{\Gamma}^*\bar{\Delta}^{-1}\bar{\sigma}^2.$$

Under the same assumption the powers are non-negative. Now set this equal to the powers given by the total load

$$((I - \tilde{L}^\dagger)\bar{G})^{-1}\tilde{L}^\dagger\bar{\sigma}^2 = (I - \bar{\Gamma}^*\bar{\Delta}^{-1}\bar{F})^{-1}\bar{\Gamma}^*\bar{\Delta}^{-1}\bar{\sigma}^2$$

and solve for $\tilde{L}^\dagger$ as a function of $\bar{\Gamma}^*$.

$$\begin{aligned} &((I - \tilde{L}^\dagger)\bar{G})^{-1}\tilde{L}^\dagger\bar{\sigma}^2 = (I - \bar{\Gamma}^*\bar{\Delta}^{-1}\bar{F})^{-1}\bar{\Gamma}^*\bar{\Delta}^{-1}\bar{\sigma}^2 \quad \Leftrightarrow \\ &\tilde{L}^\dagger\bar{\sigma}^2 = (I - \tilde{L}^\dagger)\bar{G}(I - \bar{\Gamma}^*\bar{\Delta}^{-1}\bar{F})^{-1}\bar{\Gamma}^*\bar{\Delta}^{-1}\bar{\sigma}^2 \quad \Leftrightarrow \\ &\tilde{L}^\dagger\Big(I + \bar{G}(I - \bar{\Gamma}^*\bar{\Delta}^{-1}\bar{F})^{-1}\bar{\Gamma}^*\bar{\Delta}^{-1}\Big)\bar{\sigma}^2 = \\ &\quad \bar{G}(I - \bar{\Gamma}^*\bar{\Delta}^{-1}\bar{F})^{-1}\bar{\Gamma}^*\bar{\Delta}^{-1}\bar{\sigma}^2 \end{aligned}$$

Define $\bar{M} = \bar{G}(I - \bar{\Gamma}^*\bar{\Delta}^{-1}\bar{F})^{-1}\bar{\Gamma}^*\bar{\Delta}^{-1}$. We then get $\bar{L}^\dagger$ from

$$\bar{L}_i^\dagger = \frac{\bar{M}^i\bar{\sigma}^2}{(I + \bar{M}^i)\bar{\sigma}^2}.$$

Now assume that the system is feasible with respect to given $\bar{L}^\dagger$, and solve for $\bar{\Gamma}^*$ as a function of $\bar{L}^\dagger$.

$$
\begin{aligned}
&((I-\tilde{L}^\dagger)\bar{G})^{-1}\tilde{L}^\dagger\bar{\sigma}^2 = (I-\bar{\Gamma}^*\bar{\Delta}^{-1}\bar{F})^{-1}\bar{\Gamma}^*\bar{\Delta}^{-1}\bar{\sigma}^2 \quad \Leftrightarrow\\
&(I-\bar{\Gamma}^*\bar{\Delta}^{-1}\bar{F})((I-\tilde{L}^\dagger)\bar{G})^{-1}\tilde{L}^\dagger\bar{\sigma}^2 = \bar{\Gamma}^*\bar{\Delta}^{-1}\bar{\sigma}^2 \quad \Leftrightarrow\\
&((I-\tilde{L}^\dagger)\bar{G})^{-1}\tilde{L}^\dagger\bar{\sigma}^2 - \bar{\Gamma}^*\bar{\Delta}^{-1}\bar{F}((I-\tilde{L}^\dagger)\bar{G})^{-1}\tilde{L}^\dagger\bar{\sigma}^2 =\\
&\quad \bar{\Gamma}^*\bar{\Delta}^{-1}\bar{\sigma}^2 \quad \Leftrightarrow\\
&\bar{\Gamma}^*\bar{\Delta}^{-1}\bar{\sigma}^2 + \bar{\Gamma}^*\bar{\Delta}^{-1}\bar{F}((I-\tilde{L}^\dagger)\bar{G})^{-1}\tilde{L}^\dagger\bar{\sigma}^2 =\\
&\quad ((I-\tilde{L}^\dagger)\bar{G})^{-1}\tilde{L}^\dagger\bar{\sigma}^2 \quad \Leftrightarrow\\
&\bar{\Gamma}^*\Big(\bar{\Delta}^{-1}+\bar{\Delta}^{-1}\bar{F}((I-\tilde{L}^\dagger)\bar{G})^{-1}\tilde{L}^\dagger\Big)\bar{\sigma}^2 =\\
&\quad ((I-\tilde{L}^\dagger)\bar{G})^{-1}\tilde{L}^\dagger\bar{\sigma}^2.
\end{aligned}
$$

Define $\bar{N} = ((I-\tilde{L}^\dagger)\bar{G})^{-1}\tilde{L}^\dagger$. We then get $\bar{\Gamma}^*$ from

$$\bar{\gamma}_i^* = \frac{\bar{N}^i\bar{\sigma}^2}{(\bar{\Delta}^{-1}+\bar{\Delta}^{-1}\bar{F}\bar{N})^i\bar{\sigma}^2}.$$

■

F. Proof of Proposition 8

Proof: Let us first consider the interference nonlinearity as a multivariable function $\Phi^{out} : B^*(\gamma) \to B^*(\gamma)$. It follows that

$$
\begin{aligned}
&|\Phi^{out}(x)-\Phi^{out}(y)|_\infty\\
&\quad = |\int_0^1 \nabla\Phi^{out}(y+\theta(x-y))(x-y)d\theta|_\infty\\
&\quad \le \int_0^1 |\nabla\Phi^{out}(y+\theta(x-y))|_1 d\theta |x-y|_\infty\\
&\quad \le \sup_{z\in B^*(\gamma)} |\nabla\Phi^{out}(z)|_1 |x-y|_\infty.
\end{aligned}
$$

This gives the Lipschitz bound

$$
\begin{aligned}
&L[\Phi^{out};B^*(\gamma)] \le \sup_{z\in B^*(\gamma)} |\nabla\Phi^{out}(z)|_1\\
&= \max_{z\in B^*(\gamma)} \max_i \Bigg(\frac{\bar{\sigma}_i^2\bar{F}^i e^{p^*+z}}{(\bar{G}^i e^{p^*+z}+\bar{\sigma}_i^2)(\bar{G}^i e^{p^*+z})}\\
&+ \Big| C_i - \frac{\bar{\sigma}_i^2\bar{g}_{ii}e^{p_i^*}e^{z_i}}{(\bar{G}^i e^{p^*+z}+\bar{\sigma}_i^2)(\bar{G}^i e^{p^*+z})}\Big|\Bigg).
\end{aligned}
$$

This can be seen since

$$
\begin{aligned}
\frac{\partial}{\partial z_j}\Phi_i^{out}(z) &= -\frac{\bar{\sigma}_i^2\bar{g}_{ij}e^{p_j^*}e^{z_j}}{(\bar{G}^i e^{p^*+z}+\bar{\sigma}_i^2)(\bar{G}^i e^{p^*+z})}\\
\frac{\partial}{\partial z_i}\Phi_i^{out}(z) &= -\frac{\bar{\sigma}_i^2\bar{g}_{ii}e^{p_i^*}e^{z_i}}{(\bar{G}^i e^{p^*+z}+\bar{\sigma}_i^2)(\bar{G}^i e^{p^*+z})} + C_i.
\end{aligned}
$$

Note that we can interchange the order of maximization between index i and z. We then have

$$
\begin{aligned}
&\|\Phi^{out}(z_1)-\Phi^{out}(z_2)\|_{2,\infty}\\
&\qquad = \sqrt{\sum_{k=0}^\infty |\Phi^{out}(z_1[k])-\Phi^{out}(z_2[k])|_\infty^2}\\
&\qquad \le L[\Phi^{out};B^*(\gamma)]\sqrt{\sum_{k=0}^\infty |z_1[k]-z_2[k]|_\infty^2}\\
&\qquad = L[\Phi^{out};B^*(\gamma)]\|z_1-z_2\|_{2,\infty},
\end{aligned}
$$

which shows that $L[\Phi^{out};B^*_{l_{2,\infty}}(\gamma)] \le L[\Phi^{out};B^*(\gamma)]$. We now show that the inequality in fact is an equality. Since $B^*(\gamma)\subset\mathbb{R}^n_\infty$ is compact, there exist z_1^*, z_2^* s.t. $|\Phi^{out}(z_1^*)-\Phi^{out}(z_2^*)|_\infty = L[\Phi^{out};B^*(\gamma)]|z_1^*-z_2^*|_\infty$. Equality is then reached above for the signals

$$z_1 = \begin{cases} z_1^*, & k=0\\ 0, & \text{otherwise}\end{cases}, \quad z_2 = \begin{cases} z_2^*, & k=0\\ 0, & \text{otherwise.}\end{cases}$$

The case where $\Phi^{out} : l_{2,\infty}\to l_{2,\infty}$ is analogous and hence $L[\Phi^{out};B^*_{l_{2,\infty}}(\gamma)] = L[\Phi^{out};B^*_{l_\infty}(\gamma)] = L[\Phi^{out};B^*(\gamma)]$.

Obviously Φ^{out} is continuously differentiable and the Jacobian is Lipschitz. We will now show that $L[\Phi^{out};B^*(\gamma)] = \max_{z\in B^*(\gamma)}|\nabla\Phi^{out}(z)|_1$. To see that equality can be achieved we assume

$$\max_{z\in B^*(\gamma)} |\nabla\Phi^{out}(z)|_1 := f_{i^*}(z^*),$$

where i^* is the maximizing index and z^* is the corresponding maximizing solution. We know the existence of such since $|\nabla\Phi^{out}(z)|_1$ is a continuous function and $B^*(\gamma)$ is compact. Furthermore, let δz be a unit length vector in $\mathbb{R}^n_\infty$ such that $|\nabla\Phi^{out}(z^*)\delta z|_\infty = |\nabla\Phi^{out}(z^*)|_1$. Let $\check{z}$ be an interior point of $B^*(\gamma)$ such that $|\check{z}-z^*|_\infty \le \eta$. Now let $y := \check{z}$ and $x := \check{z}-\epsilon\delta z$. We get

$$
\begin{aligned}
&\epsilon^{-1}|\Phi^{out}(x)-\Phi^{out}(y)|_\infty = |\int_0^1 \nabla\Phi^{out}(\check{z}-\epsilon\theta\delta z)\delta z d\theta|_\infty\\
&\ge |\nabla\Phi^{out}(z^*)|_1\\
&\quad - |\int_0^1 \big(\nabla\Phi^{out}(z^*)-\nabla\Phi^{out}(\check{z}-\epsilon\theta\delta z)\big)\delta z d\theta|_\infty\\
&\ge |\nabla\Phi^{out}(z^*)|_1 - (\epsilon+\eta)L[\nabla\Phi^{out};B^*(\gamma)]
\end{aligned}
$$

where $L[\nabla\Phi^{out};B^*(\gamma)]$ denotes the Lipschitz bound of the Jacobian $\nabla\Phi^{out} : B^*(\gamma)\to\mathbb{R}_1^{n\times n}$ and $\mathbb{R}_1^{n\times n}$ is the vector space of real valued $n\times n$ matrices equipped with the matrix $|\cdot|_1$-norm. Hence

$$
\begin{aligned}
&\epsilon^{-1}|\Phi^{out}(x)-\Phi^{out}(y)|_\infty\\
&\qquad \ge |\nabla\Phi^{out}(z^*)|_1 - (\epsilon+\eta)L[\nabla\Phi^{out};B^*(\gamma)],
\end{aligned}
$$

and since ϵ and η are arbitrary it follows that $L[\Phi^{out};B^*(\gamma)] \ge |\nabla\Phi^{out}(z^*)|_1$. We conclude that $L[\Phi^{out};B^*(\gamma)] = |\nabla\Phi^{out}(z^*)|_1$. ■

G. Proof of Theorem 1

Proof: We first establish that the system is a contraction under the assumptions. To prove that the system is contractive, we need to introduce a saturation. Define the saturation $\text{sat}_{[-\gamma\mathbf{1},\gamma\mathbf{1}]} : \mathbb{R}^n\to\mathbb{R}^n$ whose i^{th} component is

$$\text{sat}_{[-\gamma\mathbf{1},\gamma\mathbf{1}]}(z)_i := \begin{cases} \gamma & \text{if } z_i > \gamma\\ z_i & \text{if } -\gamma \le z_i \le \gamma\\ -\gamma & \text{if } z_i < -\gamma\end{cases}$$

and let

$$\Phi_\gamma(z) := \Phi(\text{sat}_{[-\gamma\mathbf{1},\gamma\mathbf{1}]}(z)).$$

Define $F(z) := H_1\Phi^{in}_\gamma(z) + H_2\Phi^{in}_\gamma(z) + \delta r$. Then

$$\begin{aligned}\|F(z_1) - F(z_2)\|_\infty &= \|H_1(\Phi^{in}_\gamma(z_1) - \Phi^{in}_\gamma(z_2)) \\ &\quad + H_2(\Phi^{in}_\gamma(z_1) - \Phi_{\gamma,out}(z_2))\|_\infty \\ &\le \Big(\|H_1\|_1 L[\Phi^{in}; B^*(\gamma)] \\ &\quad + \|H_2\|_1 L[\Phi^{out}; B^*(\gamma)]\Big)\|z_1 - z_2\|_\infty \\ &< \|z_1 - z_2\|_\infty, \quad \forall z_1 \neq z_2.\end{aligned}$$

Hence F is a contraction on l_∞ and according to the Banach fixed point theorem there exists a unique solution z^* to the fixed point equation $z^* = F(z^*)$. Assume now that the bound in (10) holds. Then the fixed point z^* satisfies

$$\begin{aligned}\|z^*\|_\infty &= \|F(z^*)\|_\infty = \|H_1\Phi^{in}(z^*) + H_2\Phi^{in}_\gamma(z^*) + \delta r\|_\infty \\ &\le \Big(\|H_1\|_1 L[\Phi^{in}; B^*(\gamma)] + \|H_2\|_1 L[\Phi^{out}; B^*(\gamma)]\Big)\|z^*\|_\infty \\ &\quad + \|\delta r\|_\infty\end{aligned}$$

which is equivalent to

$$\begin{aligned}&\Big(1 - \|H_1\|_1 L[\Phi^{in}; B^*(\gamma)] + \|H_2\|_1 L[\Phi^{out}; B^*(\gamma)]\Big)\|z^*\|_\infty \\ &\le \|\delta r\|_\infty\end{aligned}$$

and

$$\begin{aligned}\|z^*\|_\infty &\le \frac{\|\delta r\|_\infty}{1 - \|H_1\|_1 L[\Phi^{in}; B^*(\gamma)] + \|H_2\|_1 L[\Phi^{out}; B^*(\gamma)]} \\ &\le \gamma.\end{aligned}$$

Since $\|z^*\|_\infty \le \gamma$, there exists a unique power distribution with $\|z\|_\infty \le \gamma$ to the real system because the saturation in the definition of Φ_γ is inactive.

The last statement in the theorem follows from the bound

$$\begin{aligned}\|z^*\|_{2,\infty} \le \Big(&1 - \|H_1\|_{l_{2,\infty}\to l_{2,\infty}} L[\Phi^{in}; B^*(\gamma)] \\ &+ \|H_2\|_{l_{2,\infty}\to l_{2,\infty}} L[\Phi^{out}; B^*(\gamma)]\Big)^{-1}\|\delta r\|_{2,\infty},\end{aligned}$$

which is derived in the same fashion as the previous bound. ■

H. Proof of Proposition 9

Proof: The first statement was proved in [18] and [19] and the second follows the same lines.

Let $\hat{x} := D^{-1}x, \hat{y} := D^{-1}y$. Note that $\nabla(M\Phi^{out}(x)) = M\nabla\Phi^{out}(x)$, $M \in \mathbb{R}^{n\times n}$, and $\nabla(\Phi^{out}(Mx)) = \nabla\Phi^{out}(Mx)M$, where $\nabla\Phi^{out}(x)$ is the Jacobian of Φ^{out}. We have

$$\begin{aligned}&|\hat{\Phi}^{out}(\hat{x}) - \hat{\Phi}^{out}(\hat{y})|_\infty \\ &\quad = |\int_0^1 \nabla\hat{\Phi}^{out}(\hat{y} + \theta(\hat{x} - \hat{y}))(\hat{x} - \hat{y})d\theta|_\infty \\ &\quad = |\int_0^1 D^{-1}\nabla\Phi^{out}(D\hat{y} + D\theta(\hat{x} - \hat{y}))D(\hat{x} - \hat{y})d\theta|_\infty \\ &\quad \le \int_0^1 |D^{-1}\nabla\Phi^{out}(y + \theta(x - y))D|_1 d\theta |\hat{x} - \hat{y}|_\infty \\ &\quad \le \underbrace{\max_{z\in B^*} |D^{-1}\nabla\Phi^{out}(z)D|_1}_{:=L_D^{out}} |\hat{x} - \hat{y}|_\infty.\end{aligned}$$

where B^* is given in (8). To see that equality can be achieved we assume

$$L_D^{out} = \max_{z\in B^*} |D^{-1}\nabla\Phi^{out}(z)D|_1 := f_{i^*}(z^*),$$

where i^* is the maximizing index and z^* is the maximizing argument. Such index and argument exists, since $|D^{-1}\nabla\Phi^{out}(z)D|_1$ is a continuous function and the optimization is over a compact set. Let $\widehat{\delta z} := D^{-1}\delta z$ be a unit length vector in $\mathbb{R}^n_\infty$ such that $|D^{-1}\nabla\Phi^{out}(z^*)D\widehat{\delta z}|_\infty = |D^{-1}\nabla\Phi^{out}(z^*)D|_1$. Let $\check{z}$ be an interior point of B^* such that $|\check{z} - z^*|_\infty \le \eta$. Furthermore, let $\hat{x} := D^{-1}\check{z} - \epsilon\widehat{\delta z}$ and $\hat{y} := D^{-1}\check{z}$. We then get

$$\begin{aligned}&\frac{1}{\epsilon}|\hat{\Phi}^{out}(\hat{x}) - \hat{\Phi}^{out}(\hat{y})|_\infty \\ &\quad = \frac{1}{\epsilon}|\int_0^1 \nabla\hat{\Phi}^{out}(\hat{y} + \theta(\hat{x} - \hat{y}))(\hat{x} - \hat{y})d\theta|_\infty \\ &\quad = \frac{1}{\epsilon}|\int_0^1 D^{-1}\nabla\Phi^{out}(D\hat{y} + D\theta(\hat{x} - \hat{y}))D(\hat{x} - \hat{y})d\theta|_\infty \\ &\quad = |\int_0^1 D^{-1}\nabla\Phi^{out}(\check{z} - \theta\epsilon\delta z)D\widehat{\delta z}d\theta|_\infty \\ &\quad \ge |D^{-1}\nabla\Phi^{out}(z^*)D|_1 \\ &\quad - |\int_0^1 D^{-1}\big(\nabla\Phi^{out}(z^*) - \nabla\Phi^{out}(\check{z} - \theta\epsilon\delta z)\big)D\widehat{\delta z}d\theta|_\infty \\ &\quad \ge |D^{-1}\nabla\Phi^{out}(z^*)D|_1 - (\eta + \epsilon\tilde{d})L[D^{-1}\nabla\Phi^{out}D; B^*]\end{aligned}$$

where $\tilde{d} = \max_i d_i$ and $L[D^{-1}\nabla\Phi^{out}D; B^*]$ denotes the Lipschitz bound of the scaled Jacobian of Φ^{out}, $D^{-1}\nabla\Phi^{out}D : B^* \to \mathbb{R}^{n\times n}_1$ and $\mathbb{R}^{n\times n}_1$ is the vector space of real valued $n \times n$ matrices equipped with the matrix $|\cdot|_1$-norm. Obviously $\nabla\Phi^{out}$ is Lipschitz on B^*, and hence we have that also $D^{-1}\nabla\Phi^{out}D$ is Lipschitz. Since ϵ and η are arbitrary it follows that $L[\hat{\Phi}^{out}; D^{-1}B^*] \ge L_D^{out}$. ■